

Towards Ambiguity-Free Spatial Foundation Model: Rethinking and Decoupling Depth Ambiguity

Xiaohao Xu¹ Feng Xue¹ Xiang Li² Haowei Li¹ Shusheng Yang³
Tianyi Zhang² Matthew Johnson-Roberson² Xiaonan Huang¹

¹University of Michigan, Ann Arbor ²Carnegie Mellon University ³New York University

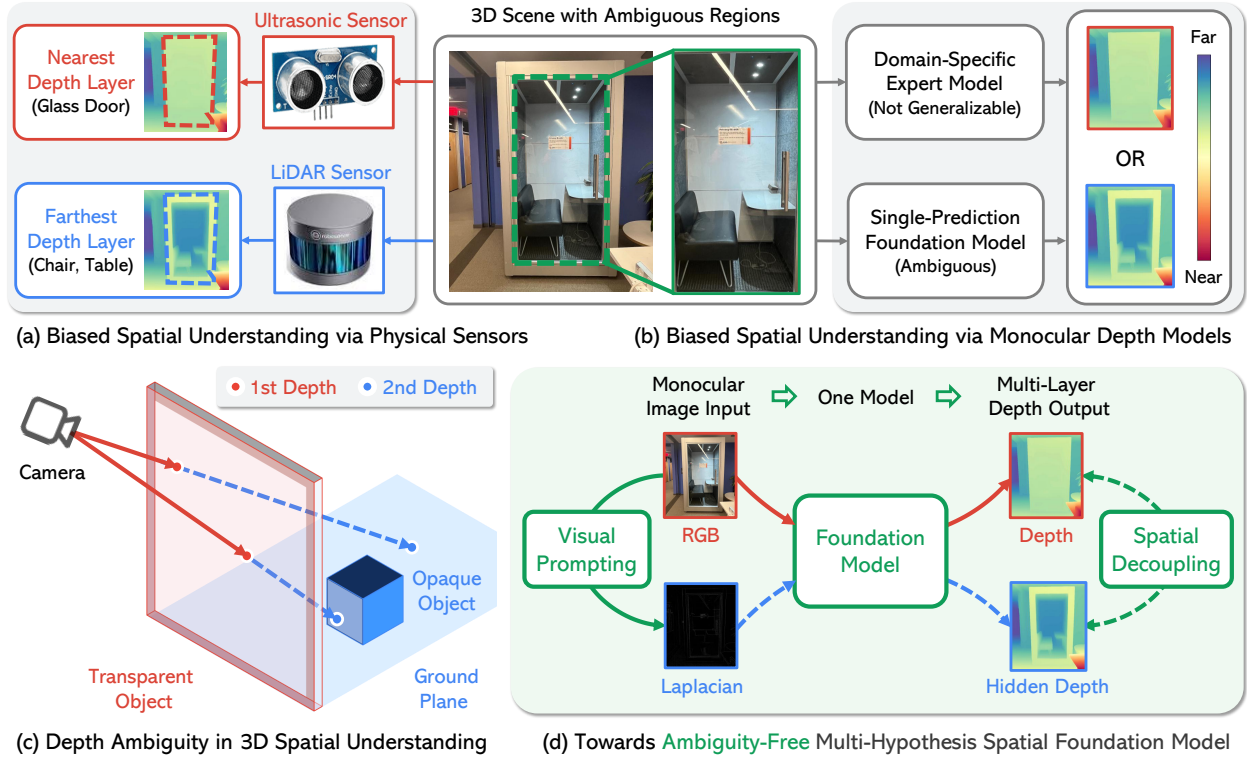


Figure 1. **Motivation.** 3D spatial understanding, powered by (a) sensors and (b) algorithms, has been confined to a biased *single-layer* representation of depth. (c) Existing methods collapse when faced with the true complexity of 3D, particularly in ambiguous scenes like those with transparency. (d) We propose Laplacian Visual Prompting (LVP) to transcend this limitation, granting *Spatial Foundation Models* the ability to derive *multi-hypothesis* depth, unlocking ambiguity-free spatial understanding.

Abstract

Depth ambiguity is a fundamental challenge in spatial scene understanding, especially in transparent scenes where single-depth estimates fail to capture full 3D structure. Existing models, limited to deterministic predictions, overlook real-world multi-layer depth. To address this, we introduce a paradigm shift from single-prediction to multi-hypothesis spatial foundation models. We first present *MD-3k*, a benchmark exposing depth biases in expert and foundational models through multi-layer spatial relationship labels and new metrics. To resolve depth ambiguity, we propose Laplacian Visual Prompting (LVP), a

training-free spectral prompting technique that extracts hidden depth from pre-trained models via Laplacian-transformed RGB inputs. By integrating LVP-inferred depth with standard RGB-based estimates, our approach elicits multi-layer depth without model retraining. Extensive experiments validate the effectiveness of LVP in zero-shot multi-layer depth estimation, unlocking more robust and comprehensive geometry-conditioned visual generation, 3D-grounded spatial reasoning, and temporally consistent video-level depth inference. Our benchmark and code will be available at <https://github.com/Xiaohao-Xu/Ambiguity-in-Space>.

1. Introduction

Spatial understanding, the ability to derive structured 3D representations from sensory data, is fundamental to visual intelligence and autonomous systems. Despite progress in both physical sensors and monocular depth estimation models [5, 6, 14, 17, 18, 20, 22, 27, 29, 38–41] (see Fig. 1a&b), a key challenge persists: **biased 3D spatial understanding under depth ambiguity**.

In real-world 3D scenes, factors such as transparency (see Fig. 1c) break the assumption that each pixel corresponds to a unique depth value. For example, objects viewed through transparent surfaces like glass exhibit a range of plausible depths rather than a single fixed value. While state-of-the-art depth foundation models [38, 39] generalize well in unambiguous scenarios, they typically output only a single depth estimate, thereby ignoring inherent depth ambiguity. This limitation results in **biased, incomplete 3D representations** that undermine both generalization and reliability, especially in safety-critical applications requiring robust spatial reasoning.

To this end, we advocate a paradigm shift from single-prediction to Multi-Hypothesis Spatial Foundation Models (MH-SFMs). We posit that **true spatial intelligence demands explicitly modeling and resolving ambiguity** rather than forcing a biased single-depth output. To address this, we propose a unified framework that enables multi-layer depth estimation from a monocular image via a single, domain-agnostic foundation model (see Fig. 1d).

To enable rigorous study of multi-layer spatial relationships under depth ambiguity, we introduce MD-3k, a benchmark featuring explicit labels for multilayer spatial relationships that goes beyond traditional single-depth metrics. Our analysis reveals that existing models exhibit significant depth biases under standard RGB input—some favoring nearer surfaces, others preferring farther ones (see Fig. 2a)—highlighting the limitations of the conventional single-depth prediction paradigm.

Next, we introduce Laplacian Visual Prompting (LVP), a training-free spectral prompting technique for 3D spatial decoupling. LVP draws inspiration from prompting techniques in NLP [37] and visual prompting [2, 3, 19]. At its core, LVP applies the discrete Laplacian operator, a fundamental second-order difference operator, to the RGB image input. This operation generates high-frequency visual prompts that highlight regions of rapid intensity change, effectively exposing latent spatial knowledge within pre-trained depth models. Integrating depth maps from LVP and RGB inputs enables multi-hypothesis depth estimation without re-training, revealing pre-trained models’ latent ability to disentangle multi-layered 3D structures. We demonstrate LVP’s effectiveness on the MD-3k benchmark, showing that it uncovers hidden depth (see Fig. 2b) and mitigates

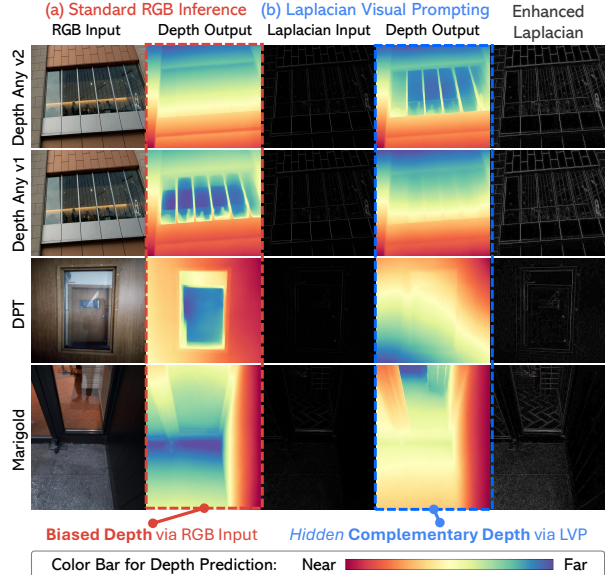


Figure 2. **Unlocking hidden depth with Laplacian Visual Prompting across diverse baselines [20, 28, 38, 39].** Each case includes the RGB input, estimated depth from RGB, Laplacian input, estimated *hidden depth* from Laplacian, and an enhanced Laplacian. Notice that depth maps from RGB and LVP **both capture plausible hypotheses**: one for the *transparent* surface (glass) and another for the *opaque* object behind it.

inherent depth biases. Further analysis using LVP explores the scaling laws of spatial understanding under ambiguous and non-ambiguous scenes, and identifies key challenges in resolving multi-layer spatial relationships.

Finally, we demonstrate the practical benefits of LVP’s multi-hypothesis depth estimation, enabling flexible geometry-conditioned visual generation [42], including realistic 3D re-synthesis of transparent structures for ambiguous scenes, consistent multi-layer depth estimation in real-world videos, and robust 3D spatial reasoning in multi-modal LLMs. These results highlight the potential of LVP in advancing spatial intelligence.

In summary, our main contributions are:

- We rethink spatial ambiguity in real-world 3D scenes and reformulate domain-agnostic, (*i.e.*, foundational) depth estimation as multi-hypothesis inference.
- We introduce MD-3k, a new benchmark to evaluate multilayer spatial understanding and model biases.
- We analyze existing models across diverse architecture, training schema, and model size on MD-3k and reveal different depth biases under ambiguity.
- We propose Laplacian Visual Prompting (LVP), a training-free prompting method, to facilitate multi-hypothesis depth estimation from pre-trained models.
- We validate LVP’s effectiveness in revealing multi-layer depth and depth bias control. We also demonstrate its benefits for geometry-conditioned visual generation, spatial reasoning, and video-level inference.

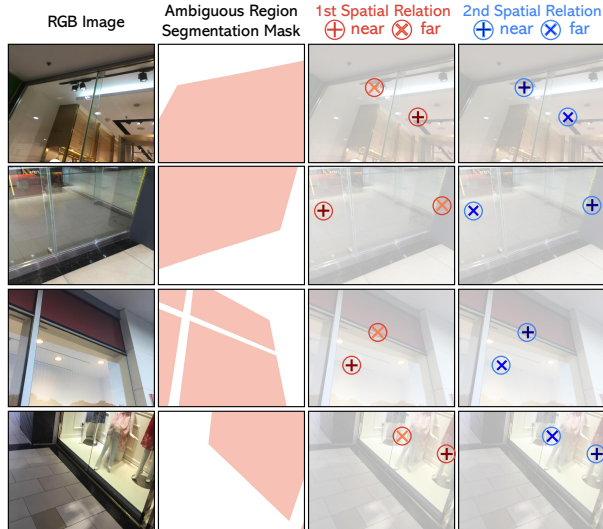


Figure 3. **MD-3k benchmark for evaluating multi-layer spatial relationships.** Example images feature annotated ambiguous region masks and sparse point pairs with multi-layer spatial labels. The first and second spatial relation columns show ground truth near/far annotations (red and blue markers, respectively). The top three rows depict *reverse* relationships, while the bottom row shows a *same* relationship between layers.

2. Related Work

Monocular depth estimation (MDE). MDE has evolved from early domain-specific depth estimation [4, 11, 13], constrained by dataset-specific training (*e.g.*, NYU [31], KITTI [16]), to more generalizable domain-agnostic approaches, pushing forward the frontier towards generic depth foundation models. Recent methods exploit Stable Diffusion [30] for fine-grained depth prediction [14, 17, 20]. MiDaS [6, 28, 29] and Metric3D [40] rely on labeled data, while Depth Anything V1 [38] and V2 [39] enhance robustness through large-scale and pseudo-labeled training. Despite these advances, *existing monocular depth foundation models estimate only single-layer depth, struggling with multi-layer spatial ambiguities.* To address this, we redefine depth estimation in a domain-agnostic setting as a multi-hypothesis problem, using Laplacian Visual Prompting to disentangle depth layers in ambiguous visual contexts.

Visual prompting (VP). Inspired by prompt-based adaptation in NLP [7], VP [1, 2] enables pre-trained vision models to be adapted via input-space manipulation. VP has been successfully applied to vision-language models [1, 32, 36], with further improvements through joint text-visual optimization [21, 35]. In addition, VP has been explored for black-box model adaptation [34], cross-domain transfer [9, 26], and adversarial robustness [8]. While VP research has primarily focused on semantic understanding tasks, *its potential for 3D spatial decoupling and comprehension remains largely unexplored.* To

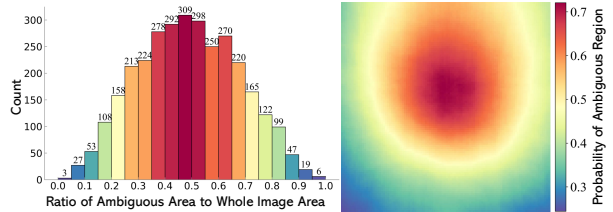


Figure 4. **Statistics of ambiguous regions in the MD-3k benchmark.** Ratio of ambiguous regions to the whole image (Left) and spatial distribution of ambiguity regions (Right)

address this gap, we introduce Laplacian Visual Prompting, which facilitates training-free spatial 3D decoupling through multi-hypothesis depth estimation.

3. Multi-Hypothesis Depth Estimation

Monocular depth estimation in complex 3D scenes is a multi-hypothesis inference problem, especially in transparent scenarios with multiple plausible depths.¹ To address this, we propose: 1) the MD-3k benchmark, which includes multi-layer spatial relationship labels, 2) new metrics for quantifying single-layer depth ambiguity and evaluating multi-layer spatial relationship accuracy, and 3) a training-free spectral prompting method, *i.e.*, Laplacian Visual Prompting, to estimate multi-layer depth.

3.1. MD-3k Benchmark: Quantifying Multi-Layer Spatial Relationships

The MD-3k benchmark quantifies spatial bias in depth estimation and evaluates multi-layer depth quality in ambiguous scenarios, providing an empirical foundation for assessing layer preference bias in pre-trained models.

Benchmark construction. MD-3k consists of 3,161 RGB images sourced from the GDD dataset [25], selected for depth ambiguity, such as transparency. Following previous spatial relationship benchmarks for non-ambiguous scenes (*e.g.*, DIW [10] and DA-2k [39]), we randomly sample a sparse point pair within the ambiguous region for each image. Expert annotators assigned pairwise depth order labels to points both on and behind transparent surfaces, generating two annotation layers. As shown in Fig. 3, each sample includes an RGB image, segmentation masks, and two types of spatial relationship labels (*near* and *far*) for point pairs representing multi-layer depths. Annotation accuracy was rigorously validated through multi-round expert review.²

Benchmark statistics. The full MD-3k dataset, referred to as *overall*, is divided into two subsets with different multi-layer spatial relationships for fine-grained analysis:

¹This work focuses on ambiguous scenes with **two** visible depth layers, leaving scenes with more than two layers for future work.

²MD-3k datasheet [15] is provided in the supplementary material.

- **Same** subset (1,783 point pairs): Consistent multi-layer relative depth ordering for each point pair.
- **Reverse** subset (1,378 point pairs): Reversed multi-layer relative depth ordering for each point pair.

These subsets facilitate the evaluation of depth estimation models under varying conditions of multi-layer spatial ambiguity and relative depth consistency.

Fig. 4 summarizes key statistics of ambiguous regions in the MD-3k benchmark. The left panel shows a histogram of the ambiguous-to-total area ratio per sample, capturing diverse ambiguity levels from minimal to near-total scene ambiguity. The right panel’s heatmap indicates a balanced spatial distribution with a slight center bias, resembling a Gaussian pattern that reflects natural scene compositions while minimizing regional biases.

3.2. Metrics: Revealing Depth Bias and Quantifying Multi-Layer Depth Accuracy

We propose metrics to capture depth prediction layer bias and quantify the accuracy of multi-layer depth estimation.

Spatial Relationship Accuracy (SRA(i)). SRA(i) measures the fraction of point pairs \mathcal{P} with correct relative depth ordering for each depth layer $i \in \{1, 2\}$:

$$\text{SRA}(i) = \frac{1}{|\mathcal{P}|} \sum_{(P_1, P_2) \in \mathcal{P}} \mathbb{I} \left(\text{sign}(\hat{d}_1^{(i)} - \hat{d}_2^{(i)}) = \text{sign}(d_1^{(i)} - d_2^{(i)}) \right), \quad (1)$$

where $\hat{d}_j^{(i)}$ and $d_j^{(i)}$ represent the predicted and ground truth depths at point P_j for layer i , respectively.

Depth Layer Preference ($\alpha(f_\theta)$). $\alpha(f_\theta)$ quantifies the bias of a depth estimation model f_θ towards one of the layers for layered scenes in its predictions. It is computed as the difference in SRA between the two layers:

$$\alpha(f_\theta) = \text{SRA}(2) - \text{SRA}(1). \quad (2)$$

A positive value, *i.e.*, $\alpha(f_\theta) > 0$, indicates a preference for the second layer, while a negative value, *i.e.*, $\alpha(f_\theta) < 0$, indicates a preference for the first layer. A larger absolute value, *i.e.*, $|\alpha(f_\theta)|$, signifies a stronger bias.

Multi-Layer Spatial Relationship Accuracy (ML-SRA). ML-SRA measures the proportion of point pairs where the predicted relative depth ordering is correct in both layers simultaneously, which is formulated as:

$$\text{ML-SRA} = \frac{1}{|\mathcal{P}|} \sum_{(P_1, P_2) \in \mathcal{P}} \mathbb{I} \left(\bigwedge_{k=1}^2 \text{sign}(\hat{d}_1^{(k)} - \hat{d}_2^{(k)}) = \text{sign}(d_1^{(k)} - d_2^{(k)}) \right). \quad (3)$$

3.3. Laplacian Visual Prompting for Multi-Layer Depth Decoupling

As shown in Fig. 5, we propose *Laplacian Visual Prompting* (LVP), a visual prompting technique designed to

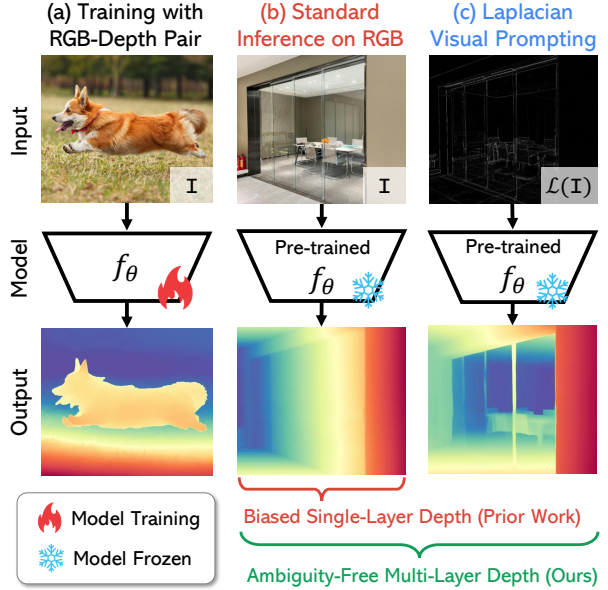


Figure 5. **Multi-layer depth with Laplacian Visual Prompting (LVP).** (a) Paired RGB-depth training of a domain-specific or domain-agnostic depth estimation model. (b) Standard inference via RGB input: single-layer depth on transparent glass. (c) Model inference via LVP: hidden depth revealing occluded objects, such as tables and chairs, behind the glass.

decouple multi-layer depth estimation by leveraging spectral components to resolve depth ambiguities in 3D scenes. LVP does not require retraining the depth model; instead, it employs a pre-trained monocular depth estimator to generate multiple depth hypotheses from a single RGB image. We posit that the latent depth distributions revealed by LVP can enhance depth estimation accuracy in scenarios with inherent depth ambiguity.

Probabilistic modeling of multi-hypotheses depth. To address depth ambiguity in monocular images, we propose a probabilistic model that predicts an ordered set of depth hypotheses, $\{\mathcal{D}_1, \mathcal{D}_2\}$, conditioned on the input image \mathcal{I} . To capture the relative depth ordering, we introduce a binary latent variable $\mathcal{O} \in \{0, 1\}$, where $\mathcal{O} = 1$ indicates that $\mathcal{D}_1 \prec \mathcal{D}_2$ (*i.e.*, \mathcal{D}_1 is closer than \mathcal{D}_2) and $\mathcal{O} = 0$ denotes that $\mathcal{D}_2 \prec \mathcal{D}_1$ (*i.e.*, \mathcal{D}_2 is closer than \mathcal{D}_1).

Rather than marginalizing over all possible orderings, we directly predict the ordered pair $(\mathcal{D}_1, \mathcal{D}_2)$ based on the sampled ordering \mathcal{O} :

$$p(\mathcal{D}_1, \mathcal{D}_2 | \mathcal{I}) = p(\mathcal{D}_1, \mathcal{D}_2 | \mathcal{O}, \mathcal{I}) p(\mathcal{O} | \mathcal{I}). \quad (4)$$

Assuming that \mathcal{D}_1 and \mathcal{D}_2 are independently estimated from \mathcal{I} and that the single-layer depth prediction model is agnostic to the ordering \mathcal{O} , we derive:

$$p(\mathcal{D}_1, \mathcal{D}_2 | \mathcal{O}, \mathcal{I}) \propto p(\mathcal{D}_1 | \mathcal{I}) p(\mathcal{D}_2 | \mathcal{I}). \quad (5)$$

Substituting into Eq. (4) yields:

$$p(\mathcal{D}_1, \mathcal{D}_2 | \mathcal{I}) \propto p(\mathcal{D}_1 | \mathcal{I}) p(\mathcal{D}_2 | \mathcal{I}) p(\mathcal{O} | \mathcal{I}), \quad (6)$$

where $p(\mathcal{D}_1 | \mathcal{I})$ and $p(\mathcal{D}_2 | \mathcal{I})$ represent the marginal likelihoods of the depth estimates for the two layers, and $p(\mathcal{O} | \mathcal{I})$ encodes the probability of the relative depth ordering. The relative ordering can be determined from the sign of layer preference $\alpha(f_\theta)$, as defined in Eq. (2).

Laplacian transformation for depth disambiguation. Monocular depth estimation often struggles with discontinuities and transparent surfaces, which leads to depth ambiguity. To mitigate this bias, we introduce Laplacian Visual Prompting, a spectral prompting strategy that uses the Laplacian operator to enhance the input image by emphasizing high-frequency details like object boundaries and edges. The Laplacian, a second-order derivative, effectively acts as a high-pass filter in the spatial domain. The 2D spatial Laplacian operator is defined as:

$$\Delta = \frac{\partial^2}{\partial x^2} + \frac{\partial^2}{\partial y^2}. \quad (7)$$

For an RGB image $\mathcal{I} \in \mathbb{R}^{H \times W \times 3}$, the Laplacian transformation is applied channel-wise:

$$\mathcal{L}(\mathcal{I}) = (\Delta\mathcal{I}_R; \Delta\mathcal{I}_G; \Delta\mathcal{I}_B), \quad (8)$$

where $\Delta\mathcal{I}_R$, $\Delta\mathcal{I}_G$, and $\Delta\mathcal{I}_B$ are the Laplacian-transformed red, green, and blue channels, respectively.

In discrete form, the Laplacian operator is approximated via a second-order finite difference scheme using a 3×3 convolution kernel:

$$\mathcal{M}_{\mathcal{L}} = \begin{bmatrix} 0 & 1 & 0 \\ 1 & -4 & 1 \\ 0 & 1 & 0 \end{bmatrix}. \quad (9)$$

Multi-hypothesis depth estimation. We apply a pre-trained monocular depth model f_θ to the original RGB image and its Laplacian-transformed version separately, which generates complementary depth hypotheses:

$$\mathcal{D}_1 = f_\theta(\mathcal{I}), \quad \mathcal{D}_2 = f_\theta(\mathcal{L}(\mathcal{I})). \quad (10)$$

These two independent depth predictions, \mathcal{D}_1 and \mathcal{D}_2 , are combined with the latent ordering probability $p(\mathcal{O} | \mathcal{I})$ as described in Eq. (4). This formulation addresses ambiguity by explicitly representing multiple depth hypotheses.

4. Experiments

To address the challenges of biased spatial understanding and unlock the potential of multi-hypothesis depth estimation, we raise the following fundamental questions: 1) **Depth bias** (Sec.4.1): In ambiguous scenes, what depth layer biases do existing models exhibit? 2) **LVP enhancement** (Sec.4.2): Can LVP effectively enhance multi-layer spatial understanding? 3) **Scaling laws** (Sec.4.3): How does model scale influence LVP-enhanced spatial understanding? 4) **Practical benefits** (Sec.4.4): What are

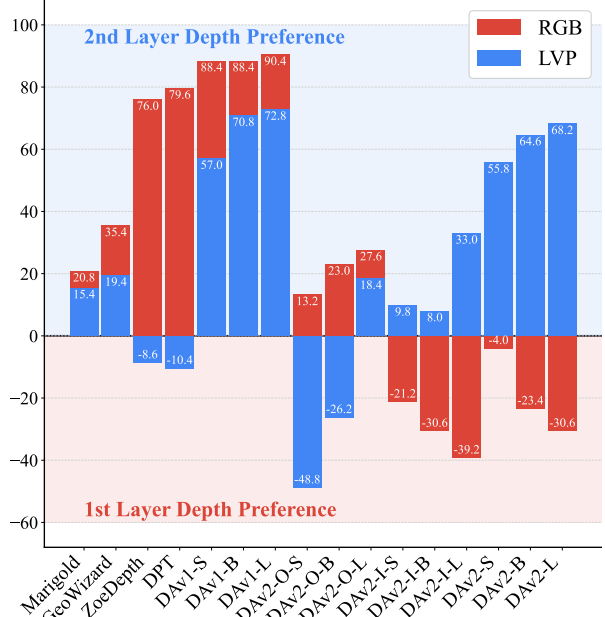


Figure 6. **Depth Layer Preference $\alpha(f_\theta)$ [%] under RGB and LVP Inputs on MD-3k (Reverse).** This figure highlights that the heterogeneous biases of standard RGB and LVP inputs significantly influence model preference, shifting it between the first and second annotated depth layers for certain models. This demonstrates how input modality can alter depth layer bias.

the practical advantages of LVP-driven multi-hypothesis depth? 5) **LVP design** (Sec.4.5): How do LVP’s design choices impact performance under ambiguity?

Baseline models. We assess bias and evaluate the effectiveness of our proposed multi-hypothesis depth estimation method via LVP across diverse baseline models, including Depth Anything V1/V2 (DAv1/2-S,B,L with ViT backbones [38, 39]). These models include general (DAv1/2), indoor (DAv2-I), and outdoor (DAv2-O) fine-tuned variants. Additional models include the discriminative models DPT [28] and ZoeDepth [5], as well as the generative models Marigold [20] and GeoWizard [14].

4.1. Probing Single-Layer Depth Prediction Bias

We first analyze depth layer preference bias, which is defined in Eq. (2), for baseline models, revealing inherent biases in predicting closer or farther surfaces in ambiguous regions using standard RGB input. We then explore whether LVP can alter these biases by introducing complementary depth hypotheses to enrich RGB predictions.

Heterogeneous depth layer bias under standard RGB input. In Fig. 6, we observe significant heterogeneity in depth layer prediction preferences across models. Some models (e.g., DAv2, DAV2-I) exhibit a bias towards the first depth layer, i.e., $\alpha(f_\theta) < 0$, while others favor the second depth layer. In addition, models with the same architecture fine-tuned on different datasets (in-

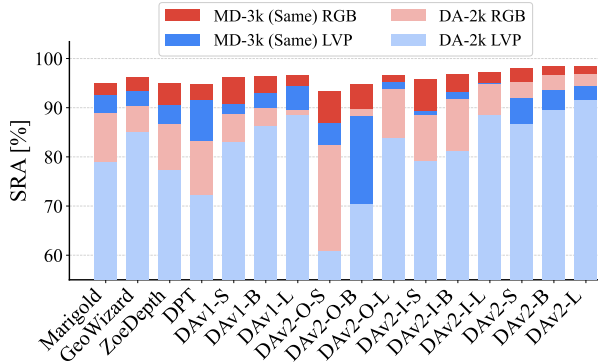


Figure 7. **High Spatial Relationship Accuracy (SRA) [%] under RGB and LVP inputs on the *same* subset of MD-3k and DA-2k [39]** (non-ambiguous benchmark for reference).

door/outdoor) can exhibit opposing depth biases, *e.g.*, DAV2-I and DAV2-O. This highlights how training data can hardwire assumptions about scene structure.

LVP modulates depth prediction preference. Comparing RGB and LVP results in Fig. 6 reveals that LVP effectively *reverses* or *attenuates* depth preferences across all baseline models. The pronounced impact of LVP on depth preference modification, particularly in models like DAV2, suggests its ability to unlock latent representations. This reveals previously suppressed depth layers and fundamentally reshapes the model’s depth interpretation.

True depth ambiguity exposes depth biases and remains challenging to tackle. True depth ambiguity, exemplified by scenes with *reverse* multi-layer spatial relationships (see Fig. 6), critically reveals depth layer biases. In these ambiguous scenarios, performance becomes inconsistent (*i.e.*, large $|\alpha(f_\theta)|$) across RGB and LVP inputs, highlighting the difficulty in resolving conflicting spatial cues. Conversely, in non-ambiguous scenes with *same* multi-layer relationships (see Fig. 7), models achieve consistently high performance, exceeding 85% SRA under RGB input. This robustness is further supported by the small performance gap between RGB and LVP inputs on the non-ambiguous DA-2k benchmark, and the comparable RGB performance observed between MD-3k (*same*) and DA-2k. Thus, ambiguous scenes with *reverse* multi-layer relationships serve as a crucial diagnostic tool, effectively exposing the inherent depth biases and limitations of current depth baseline models.

4.2. Multi-Layer Spatial Relationship Accuracy

Fig. 8 shows the Multi-Layer Spatial Relationship Accuracy (ML-SRA) achieved by our multi-hypothesis depth estimation method, which combines depth estimates from both RGB images and LVP inputs. This evaluation demonstrates the effectiveness of Laplacian Visual Prompting in generating complementary depth hypotheses beyond RGB-based inference, enabling ambiguity-

	(a) Overall	(b) Reverse	(c) Same	
Marigold	57.4	15.3	89.8	ML-SRA [%]
GeoWizard	59.5	17.6	91.9	
ZoeDepth	68.8	45.4	86.8	
DPT	70.2	46.4	88.7	
DAv1-S	57.9	17.7	89.0	
DAv1-B	56.6	11.4	91.5	
DAv1-L	57.1	10.9	92.8	
DAv2-O-S	63.0	36.6	83.5	
DAv2-O-B	62.7	32.9	85.6	
DAv2-O-L	60.4	17.6	93.4	
DAv2-I-S	60.9	27.7	86.5	
DAv2-I-B	63.7	28.1	91.2	
DAv2-I-L	71.1	42.5	93.2	
DAv2-S	67.2	36.9	90.7	
DAv2-B	73.3	48.2	92.7	
DAv2-L	75.5	52.2	93.6	

Figure 8. **Multi-Layer Spatial Relationship Accuracy (ML-SRA) [%] of our LVP-empowered multi-layer depth on MD-3k.** Effective performance gains of LVP-derived multi-depth over random guess (25%) are highlighted in green boxes.

free spatial understanding across diverse baselines.

Latent multi-layer knowledge suggests potential for MH-SFMs, unlocked by LVP. Despite being trained on single-layer depth data, some models implicitly capture multi-layer spatial relations. For example, DAV2, ZoeDepth, and DPT, when prompted with LVP, achieve non-trivial ML-SRA scores in challenging reverse spatial relationships (see Fig. 8b). This demonstrates that LVP effectively elicits this latent knowledge, suggesting that these models have the potential to be adapted into MH-SFMs, capable of representing and reasoning about multiple depth hypotheses. The fact that LVP is able to unlock this hidden potential highlights its significance as a key enabler for multi-hypothesis depth estimation.

Challenges in reverse relationships highlight the need for explicit ambiguity modeling, even with LVP. Accurately resolving depth ambiguity in *reverse* multi-layer spatial relationships remains challenging, even when using LVP to generate multi-layer depth estimates. The performance gap between *same* and *reverse* relationships highlights the difficulty of handling conflicting spatial cues and the limitations of relying solely on implicit priors, even when augmented by LVP. The reduced ML-SRA of domain-finetuned DAV2 models further suggests that optimizing for single-domain performance can hinder generalization to multi-layer scenes, reinforcing the need for models that can explicitly model and resolve ambiguity, rather than relying on domain-specific heuristics, even when combined with LVP-based prompting.

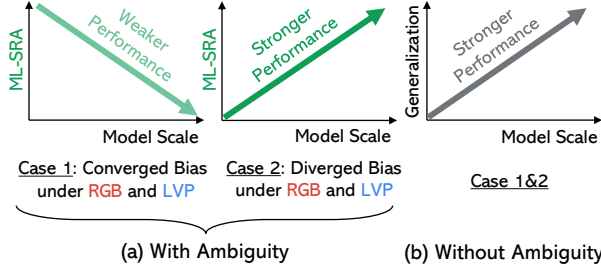


Figure 9. **Scaling laws of spatial understanding: performance trends in ambiguous vs. non-ambiguous scenes.** (a) In ambiguous scenes, converged depth bias (Case 1) leads to weaker performance with scale, while diverged bias (Case 2) yields stronger performance. (b) In non-ambiguous scenes, performance consistently improves with model scale, showing stronger generalization to the *out-of-distribution* LVP input.

4.3. Scaling Laws of Spatial Understanding

Developing generalist foundation models requires understanding performance scaling [2, 12]. We investigate how model scale impacts depth layer bias, multi-layer depth estimation in ambiguous scenes, and single-layer depth estimation in non-ambiguous scenes using Laplacian Visual Prompting (LVP), providing insights for building more reliable large-scale spatial foundation models.

To provide a high-level overview of these scaling behaviors, Fig. 9 summarizes the key performance trends observed in both ambiguous and non-ambiguous scenes as model scale increases. As depicted, **the impact of model scaling on spatial understanding is nuanced and context-dependent, echoing a concurrent work on multi-modal alignment** [33]. Specifically, in ambiguous scenes, we observe divergent performance scaling depending on whether the model exhibits *converged* or *diverged* depth bias under RGB and LVP inputs. This divergence suggests that in scenarios with high spatial ambiguity (akin to high *uniqueness* in multi-modal data [33]), simply increasing model scale does not uniformly translate to improved performance. Instead, the *nature* of representation learning, specifically the depth bias, becomes a critical factor. Conversely, in non-ambiguous scenes, a more consistent pattern of generalization improvement with scale emerges, aligning with the expected benefits of larger model capacity in less challenging scenarios where redundancy is higher and ambiguity is lower.

Model scale amplifies depth layer preference bias under RGB input. As shown in the left panel of Fig. 10, larger models tend to exhibit a stronger preference for certain depth layers under RGB input in ambiguous scenes with *reverse* multi-layer spatial relationships. DAV1 and DAV2-O models demonstrate a growing preference for the second depth layer while DAV2 and DAV2-I models demonstrating an increasing preference for the first layer. **Divergent depth bias elicit stronger multi-layer depth**

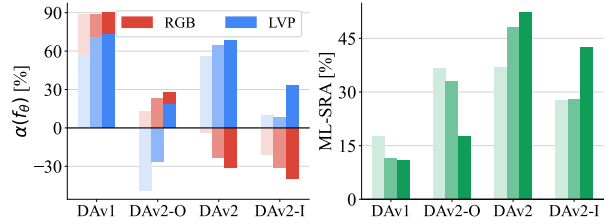


Figure 10. **Performance in ambiguous scenes (MD-3k reverse subset) as model scale increases.** **Left:** Depth Layer Preference $\alpha(f_\theta)$ [%]. **Right:** Multi-Layer Spatial Relationship Accuracy (ML-SRA) [%]. Bars within each group represent small, base, and large model variants (left to right).

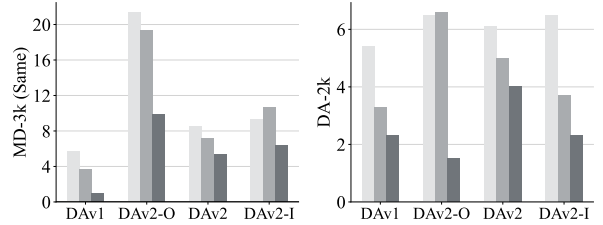


Figure 11. **Generalization to LVP input in non-ambiguous scenes as model scale increases,** measured by the SRA [%] gap between RGB and LVP inputs on the *same* subset of MD-3k (Left) and the non-ambiguous benchmark DA-2k (Right).

prediction with scale. As shown in the right panel of Fig. 10, larger models can exhibit a stronger divergence in depth layer preference based on input modality (RGB vs. LVP) in ambiguous scenes. Some models (DAV1, DAV2-O) *converge* towards a consistent second-layer preference, reducing multi-layer accuracy. Others (DAV2, DAV2-I) show a *divergence*, improving ML-SRA with larger model, suggesting more diverse latent representations that encode multiple depth hypotheses.

Enhanced generalization with increasing model scale in non-ambiguous scenes. Fig. 11 shows the performance gap between RGB and LVP inputs narrows as model scales. This improved generalization is observed in both multi-layer scenes with *same* spatial relationships of MD-3k and non-ambiguous scenes of DA-2k.

Implications for Generalist Spatial Foundation Models. Scaling model size alone is insufficient for MH-SFMs. A nuanced approach, considering model capacity, scene ambiguity, and depth bias, is essential. For ambiguous scenes, representational diversity and bias mitigation may be more effective than simply increasing parameters, while scaling is beneficial for less ambiguous tasks.

4.4. Applications of Multi-Hypothesis Depth

The multi-hypothesis depth predictions enabled by LVP enhance 3D-conditional image generation for ambiguous scenes. This capability supports the creation of complex environments, such as those featuring both transparent and opaque objects (*e.g.*, glass doors and windows), using geometry-conditioned ControlNet [42] (see Fig. 12).

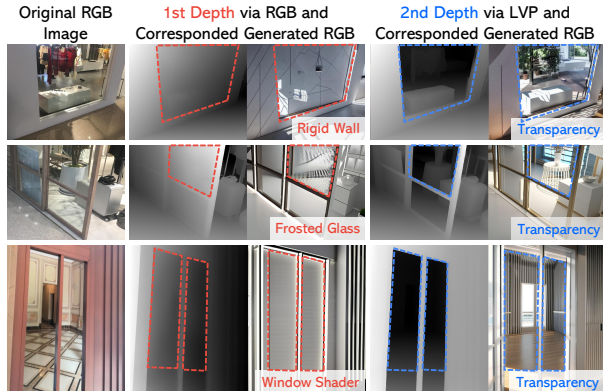


Figure 12. Flexible 3D-conditioned visual generation.



Figure 13. Robust 3D spatial reasoning with LLM.

In addition, LVP boosts 3D spatial reasoning through a Multi-modal Large Language Model (LLM), exemplified by precise 3D-grounded human counting with the ChatGPT o3-mini model (see Fig. 13). Furthermore, the multi-layer depth estimation underlying these predictions also demonstrates robust consistency when applied to real-world complex videos, as evidenced in Fig. 14.³

4.5. Ablation Study of LVP Design

Fig. 15 shows that ML-SRA performance is largely unaffected by Laplacian discretization (4-neighbor vs. 8-neighbor in LVP and LVP-2) and kernel sign (LVP-R with reversed convolution vs. LVP), with variations generally within $\pm 3\%$. While grayscale LVP (LVP-G) slightly reduces SRA compared to RGB LVP, the difference is minimal. These results highlight the crucial role of high-frequency information in 3D spatial decoupling.

5. Conclusion

We redefine domain-agnostic monocular spatial foundation models as inherently ambiguous, multi-hypothesis problems. To advance this, we introduce Laplacian Visual Prompting (LVP), a training-free technique for multi-layer depth estimation, and MD-3k, the first benchmark

³For implementation details and additional qualitative results (including the video demo), please refer to our supplementary material.

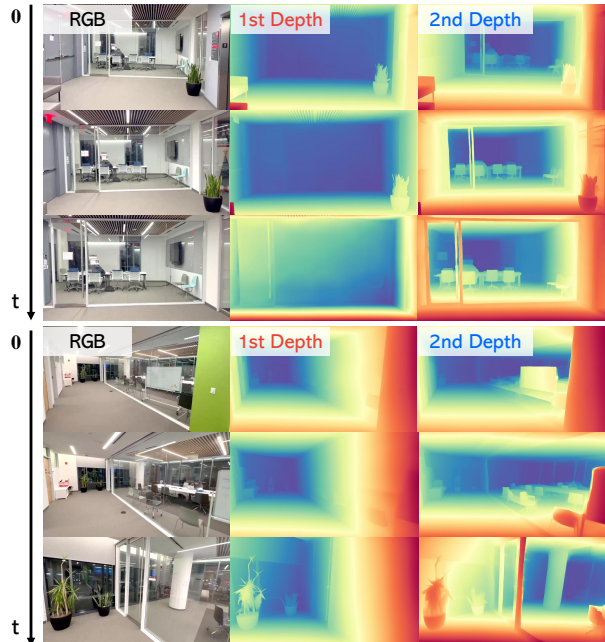


Figure 14. Consistent multi-layer depth estimation on video.

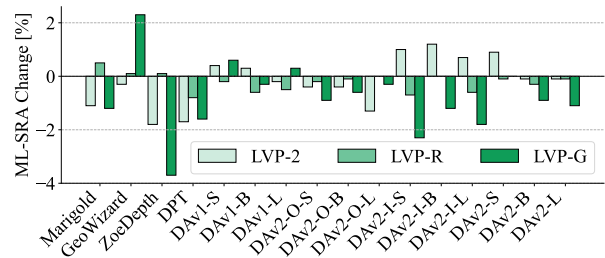


Figure 15. Ablation study of LVP design. Overall ML-SRA [%] change relative to the default LVP on MD-3k is shown.

for evaluating multi-layer depth under ambiguity. Our analysis highlights significant biases in existing models, revealing the limitations of single-depth estimation. Experiments show that LVP modulates depth biases, enables comprehensive multi-layer estimation, and enhances downstream task robustness and flexibility.

Limitation & future work. Future work should explore spatial understanding with a wider range of multi-modal visual prompts, such as learned spectral transformations. While our MD-3k benchmark leverages real-world images containing inherent noise, it is important to evaluate the robustness of LVP under various noise and artifact conditions. Moreover, extending our benchmark to incorporate real-world multi-layer depth annotations—potentially through the integration of multiple physical sensors—would provide a more comprehensive metric for assessing multi-layer depth performance, though this remains a challenging task. Finally, to enable reliable spatial foundation models, future research could explore how to address and characterize more diverse spatial ambiguity, *e.g.*, reflection effects.

Towards Ambiguity-Free Spatial Foundation Model: Rethinking and Decoupling Depth Ambiguity

Supplementary Material

A. More Qualitative Results

Multi-layer depth decoupling with Laplacian Visual Prompting. In addition to demonstrating the effectiveness of LVP in revealing hidden depth layers in various models (Fig. A), we further demonstrate its capabilities using the best-performing baseline model, *i.e.*, the Depth Anything v2-Large (DAv2-L) model, in Figures E through J. LVP effectively elicits alternative depth hypotheses, particularly in scenes with transparency and occlusion. Although conventional depth estimations often fail to capture the layered nature of these scenes, collapsing multiple depths into a single layer, Laplacian-prompted depth maps reveal previously hidden depth layers, clearly delineating transparent surfaces and occluded objects behind the transparent surfaces.

Failure cases in multi-layer depth decoupling with Laplacian Visual Prompting. Despite significant improvements in multi-layer depth estimation, Laplacian Visual Prompting (LVP) is not immune to failure cases, especially due to its training-free nature. We present these failures in Fig. K. One type occurs when the initial single-layer depth prediction from the RGB input is already incorrect. In these instances, LVP struggles to correct the depth bias, resulting in inaccurate multi-layer depth predictions. This is particularly problematic when the RGB model’s depth map contains errors in ambiguous regions, limiting LVP’s ability to produce accurate alternative depth hypotheses. The second type of failure happens when LVP predicts a depth layer similar to the RGB output, failing to decouple distinct depth layers. This occurs when LVP cannot extract sufficient high-frequency information from the Laplacian mask to differentiate between near and far surfaces, especially in scenes with low depth contrast or complex occlusions. These cases highlight the challenges in multi-layer depth estimation, underscoring the need for improved baseline foundation models and refined prompts.

Additional MD-3k benchmark samples. Fig. L presents additional examples from the MD-3k benchmark, our newly introduced data set to evaluate the understanding of multi-layer spatial relationships. These examples highlight the diverse and challenging scenarios within MD-3k, including varying levels of depth ambiguity and transparency. By providing a broader range of scenes, we aim to assess how well models can disambiguate depth layers in multi-layered environments, particularly in real-world images that reflect the complex-

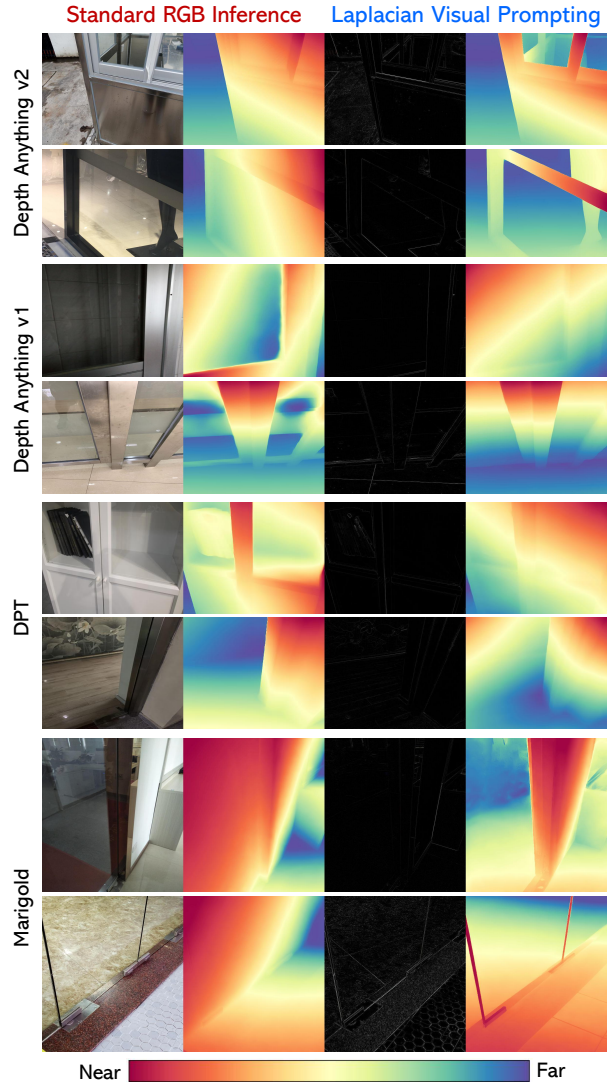


Figure A. **Unlocking hidden depth with Laplacian Visual Prompting on diverse models [20, 28, 38, 39].** Each case shows the RGB input, the estimated depth via RGB, the Laplacian input, and the estimated *depth* via Laplacian input.

ities and nuances of natural scenes.

Privacy-preserving potential of Laplacian visual prompts in non-ambiguous scenes. Fig. B demonstrates that relative depth estimation using Laplacian-transformed visual prompts closely matches results obtained from standard RGB images in unambiguous scenes, highlighting LVP’s strong generalization ability. This characteristic enables privacy-preserving applica-

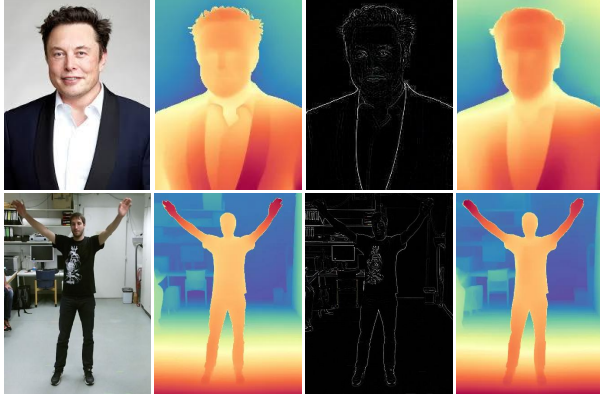


Figure B. **Privacy-preserving potential of LVP.** Depth estimation results on non-ambiguous scenes using LVP are comparable to those using original RGB input. Each example shows the RGB image and its depth, alongside the Laplacian-transformed image and its corresponding depth.

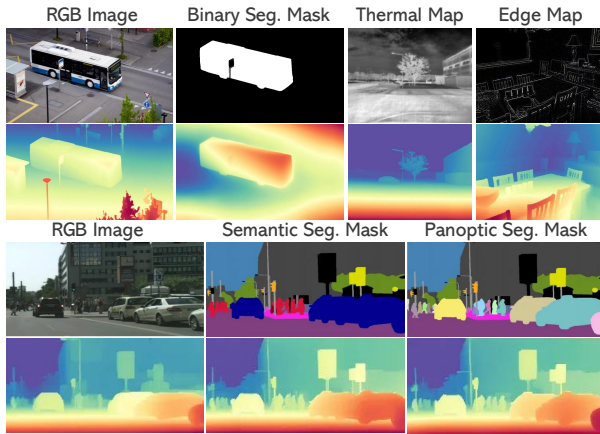


Figure C. **Generalization of depth prediction to diverse high-frequency visual prompts beyond Laplacian input,** including segmentation masks, thermal maps, and edge maps.

tions by allowing only the Laplacian-transformed image to be transmitted to a cloud-based depth foundation model, thereby avoiding the transmission of sensitive low-level image features that could reveal human identities. Furthermore, Fig. C illustrates that this property extends to various high-frequency visual prompts. Combined with the spatial decoupling findings in our main paper, LVP ensures depth prediction invariance in unambiguous scenes while enabling spatial decoupling in ambiguous ones, advancing the development of ambiguity-aware spatial foundation models.

B. More Quantitative Results

LVP enables training-free multi-layer depth, approaching performance with semantic priors, highlighting its effectiveness. Table A shows that the LVP-powered model (DAv2-L as baseline) achieves ML-SRA

Method	Semantics	Overall	Reverse	Same
LVP (Default)	No	75.5	52.2	93.6
+ Predicted Mask †	Yes	75.8	55.2	91.6
+ GT Mask (Ideal)	Yes	82.5	69.2	92.7

† Overall predicted mask quality on MD-3k: 0.8815 in mean IoU.

Table A. Even without using any extra semantic priors, our LVP-empowered multi-layer depth achieves comparable performance (measured by ML-SRA [%]) to multi-layer depth interpolation using semantic priors (predicted mask from [24]).

comparable to methods utilizing semantic priors, such as predicted segmentation masks. This demonstrates LVP’s ability to leverage the model’s implicit spatial understanding for spatial decoupling, without the need for domain-specific knowledge or post-processing, positioning it as a key component in developing generic MH-SFMs.

Our semantics-guided approach to multi-layer depth estimation integrates monocular depth predictions with semantic segmentation. We use the Depth Anything v1 Large model (DAv1-L) [38] for initial single-layer depth estimation. As noted in the main paper, DAV1-L tends to predict greater depths in ambiguous regions. Building on this bias, we estimate the nearer depth layer, typically corresponding to transparent surfaces, by interpolating depth values from the boundaries of ambiguous regions. This process is guided by a segmentation mask of the transparent surface and informed by DAV1-L’s depth estimates outside the ambiguous regions.

Figures M and N present qualitative results, showcasing both successful and failure cases. While this hybrid approach, combining DAV1-L’s depth bias with semantic segmentation, achieves higher quantitative precision for multi-layer depth estimation than our training-free LVP method, we emphasize the importance of developing foundational models that can directly handle multi-layer depth estimation, rather than relying on task-specific model combinations.

Detailed benchmarking results on MD-3k. Table B presents per-layer Spatial Relationship Accuracy (SRA) [%] for various baseline models on the MD-3k benchmark and the DA-2k dataset (non-ambiguous reference) for future comparison.

Detailed ablation study results of Laplacian Visual Prompting design on MD-3k. Table C presents ML-SRA performance under different Laplacian discretization (4-neighbor vs. 8-neighbor in default LVP and LVP-2), kernel sign (LVP-R with reversed convolution vs. LVP), and color space (RGB vs. grayscale, LVP vs. LVP-G). The results show that ML-SRA performance remains largely unaffected, highlighting the crucial role of high-frequency information in 3D spatial decoupling.

Baseline	(a) MD-3k (Overall Set)				(b) MD-3k (Reverse Subset)				(c) MD-3k (Same Subset)		(d) DA-2k	
	RGB Input		LVP Input		RGB Input		LVP Input		RGB	LVP	RGB	LVP
	SRA(1)	SRA(2)	SRA(1)	SRA(2)	SRA(1)	SRA(2)	SRA(1)	SRA(2)	SRA(1/2)	SRA(1/2)	SRA	SRA
Random	50.0	50.0	50.0	50.0	50.0	50.0	50.0	50.0	50.0	50.0	50.0	50.0
Marigold	70.7	79.9	70.8	77.4	39.6	60.4	42.3	57.7	95.0	92.6	88.9	78.9
GeoWizard	68.3	83.8	70.3	78.7	32.3	67.7	40.3	59.7	96.2	93.4	90.3	85.0
ZoeDepth	58.7	92.6	74.6	70.9	12.0	88.0	54.3	45.7	94.9	90.4	86.7	77.2
DPT	58.0	91.9	75.7	71.1	10.2	89.8	55.2	44.8	94.8	91.5	83.2	72.2
DAv1-S	56.8	95.3	60.6	85.4	5.8	94.2	21.5	78.5	96.1	90.7	88.7	83.0
DAv1-B	56.8	95.4	58.8	89.7	5.8	94.2	14.6	85.4	96.3	93.0	89.9	86.2
DAv1-L	56.6	96.0	59.2	90.9	4.8	95.2	13.6	86.4	96.6	94.3	89.5	88.5
DAv2-O-S	71.6	77.3	81.4	60.1	43.4	56.6	74.4	25.6	93.3	86.8	82.3	60.9
DAv2-O-B	70.3	80.3	77.2	65.8	38.5	61.5	63.1	36.9	94.8	88.2	89.7	70.4
DAv2-O-L	70.4	82.4	71.5	79.5	36.2	63.8	40.8	59.2	96.7	95.2	93.7	83.8
DAv2-I-S	80.4	71.2	70.0	74.3	60.6	39.4	45.1	54.9	95.8	89.3	88.5	79.2
DAv2-I-B	83.1	69.7	72.6	76.1	65.3	34.7	46.0	54.0	96.8	93.1	91.8	81.1
DAv2-I-L	85.2	68.1	68.1	82.6	69.6	30.4	33.5	66.5	97.3	95.0	94.8	88.4
DAv2-S	78.0	76.2	61.5	85.8	52.0	48.0	22.1	77.9	98.0	91.9	95.1	86.6
DAv2-B	82.4	72.3	60.5	88.6	61.7	38.3	17.7	82.3	98.5	93.5	96.7	89.5
DAv2-L	84.0	70.6	60.2	89.9	65.3	34.7	15.9	84.1	98.5	94.4	96.9	91.5

Table B. Spatial Relationship Accuracy (SRA) [%] for diverse baseline models on (a-c) the MD-3k benchmark and (d) the DA-2k dataset (non-ambiguous reference). SRA(1) and SRA(2) measure the accuracy between the model’s single-layer depth estimate and the first and second layer annotation labels, respectively; higher values indicate a preference for that layer. Input modality (RGB or LVP) yielding higher SRA(1) or SRA(2) per model on the full overall set and reverse subset of MD-3k are bolded.

C. Implementation Details

C.1. Laplacian Visual Prompting for Sequential Video Inference

We introduce Laplacian Visual Prompting (LVP) for sequential video inference, specifically for multi-layer depth estimation. Using the Video Depth Anything model as our baseline, LVP follows the multi-hypothesis depth estimation framework outlined in the main paper. Crucially, LVP enhances temporal consistency in depth estimation, mitigating inconsistencies common in per-frame processing. Additionally, the extracted hidden depth maps maintain high fidelity throughout the video sequence. A video demonstration is provided in the supplementary material.

C.2. Depth-Conditioned Image Generation

Our image generation pipeline uses depth maps and text prompts to guide scene synthesis. Depth maps are estimated using our proposed method, ensuring geometric accuracy, while text prompts modulate the visual attributes of the generated images.

We employ two distinct text prompts to control the scene’s appearance:

- a bright, well-lit photograph of an interior space with natural daylight, clear windows, balanced lighting, accurate geometry and structure, photorealistic, vibrant colors, modern interior design, clean and airy space

The resulting RGB images, synthesized from multi-layer depth representations derived via LVP, are illustrated in Fig. O.

- a bright, well-lit photograph of an interior space, accurate geometry and structure, photorealistic, modern interior design, clean and airy space

The corresponding RGB images, generated using multi-layer depth representations from LVP, are presented in Fig. P.

These prompts enhance photorealistic scene synthesis by ensuring precise geometry and well-balanced lighting, complementing depth information. More details on the diffusion models used for depth-conditioned visual generation are available in the *Diffusers* library⁴.

⁴<https://huggingface.co/docs/diffusers/en/>

Baseline	LVP (Default)	LVP-2	LVP-R	LVP-G
Random	25.0	25.0	25.0	25.0
Marigold	57.4	56.3 (-1.1)	57.9 (+0.5)	56.2 (-1.2)
GeoWizard	59.5	59.2 (-0.3)	59.6 (+0.1)	61.8 (+2.3)
ZoeDepth	68.8	67.0 (-1.8)	68.9 (+0.1)	65.1 (-3.7)
DPT	70.2	68.5 (-1.7)	69.4 (-0.8)	68.6 (-1.6)
DAv1-S	57.9	58.3 (+0.4)	57.7 (-0.2)	58.5 (+0.6)
DAv1-B	56.6	56.9 (+0.3)	56.0 (-0.6)	56.3 (-0.3)
DAv1-L	57.1	56.9 (-0.2)	56.6 (-0.5)	57.4 (+0.3)
DAv2-O-S	63.0	62.6 (-0.4)	62.8 (-0.2)	62.1 (-0.9)
DAv2-O-B	62.7	62.3 (-0.4)	62.6 (-0.1)	62.1 (-0.6)
DAv2-O-L	60.4	59.1 (-1.3)	60.4 (-0.0)	60.1 (-0.3)
DAv2-I-S	60.9	61.9 (+1.0)	60.2 (-0.7)	58.6 (-2.3)
DAv2-I-B	63.7	64.9 (+1.2)	63.7 (-0.0)	62.5 (-1.2)
DAv2-I-L	71.1	71.8 (+0.7)	70.5 (-0.6)	69.3 (-1.8)
DAv2-S	67.2	68.1 (+0.9)	67.1 (-0.1)	67.2 (-0.0)
DAv2-B	73.3	73.2 (-0.1)	73.0 (-0.3)	72.4 (-0.9)
DAv2-L	75.5	75.4 (-0.1)	75.4 (-0.1)	74.4 (-1.1)

Table C. Ablation study of LVP design via ML-SRA [%].

D. Datasheet for MD-3k Benchmark

We document the necessary information about the proposed datasets and benchmarks following the guidelines of Gebru *et al.* [15].

D.1. Motivation

Q1 **For what purpose was the dataset created?** Was there a specific task in mind? Was there a specific gap that needed to be filled? Please provide a description.

- Fig. D highlights the limitations of existing datasets for ambiguous transparent scenes. They often contain noisy raw depth from sensors (due to physical limitations) and inaccurate curated depth (due to human error). These challenges motivate our creation of the MD-3k benchmark.
- Our benchmark was created to evaluate multi-layer spatial perception, specifically focusing on the challenge of depth disentanglement in ambiguous 3D scenes. Existing depth datasets lack multi-layer spatial relationship labels, hindering fine-grained analysis in regions with transparency and spatial ambiguity. MD-3k fills this gap by providing the first benchmark with multi-layer spatial relationship labels, enabling detailed evaluation of models' ability to understand layered depth ordering.

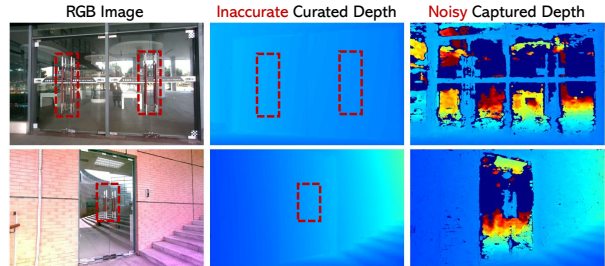


Figure D. Noise and inaccuracies in depth data from existing datasets [23] for complex, ambiguous scenes. These arise from limitations in both sensor acquisition and human annotation.

Q2 **Who created the dataset (e.g., which team, research group) and on behalf of which entity (e.g., company, institution, organization)?**

- This benchmark is presented by [Anonymous Author]⁵. Our aim is to advance the development and evaluation of spatial perception models, particularly in understanding multi-layer depth relationships in complex scenes.

Q3 **Who funded the creation of the dataset?** If there is an associated grant, please provide the name of the grantor and the grant name and number.

- This work was partially supported by [Anonymous Author].

Q4 **Any other comments?**

- No.

D.2. Composition

Q5 **What do the instances that comprise the dataset represent (e.g., documents, photos, people, countries)?** Are there multiple types of instances (e.g., movies, users, and ratings; people and interactions between them; nodes and edges)? Please provide a description.

- The instances in MD-3k represent high-resolution RGB images of indoor and outdoor scenes containing ambiguous regions, particularly those involving transparent objects. Each instance is associated with segmentation masks highlighting ambiguous regions and pairwise spatial relationship labels for sparse points within these regions.

Q6 **How many instances are there in total (of each type, if appropriate)?**

- The MD-3k benchmark comprises 3,161 high-resolution RGB images. Each image contains annotations of spatial relationships for pairs of sparse points in ambiguous regions, totaling 3,161 annotated pairs. For each pair, two spatial relationship

⁵Author and repository information have been anonymized in compliance with the double-blind policy and will be provided upon acceptance.

labels are provided, representing the relationship ‘on’ and another for the region ‘behind’ the transparent object.

Q7 Does the dataset contain all possible instances or is it a sample (not necessarily random) of instances from a larger set? *If the dataset is a sample, what is the larger set? Is the sample representative of the larger set (e.g., geographic coverage)? If so, please describe how this representativeness was validated/verified. If it is not representative of the larger set, please describe why not (e.g., to cover a more diverse range of instances, because instances were withheld or unavailable).*

- The dataset is a carefully selected sample from the GDD segmentation dataset [25]. The larger set is the entire GDD dataset. The sample is not random but specifically chosen to include scenes rich in ambiguous regions, particularly those with transparent objects, to address the benchmark’s focus on multi-layer spatial understanding in such challenging scenarios.

Q8 What data does each instance consist of? *“Raw” data (e.g., unprocessed text or images) or features? In either case, please provide a description.*

- Each instance consists of:
 - **RGB image:** High-resolution (720p) RGB image in PNG format.
 - **Segmentation masks:** Binary masks highlighting ambiguous regions within the RGB image, in PNG format.
 - **Spatial relationship labels:** Pairwise spatial relationship labels for sparse points in ambiguous regions, provided in JSON format. Each pair has two labels: one for the region ‘on’ and another for the region ‘behind’ the transparent object, indicating depth ordering (above and behind).

This data is considered ‘raw’ in the sense that it is primarily image data and annotations, not pre-extracted features.

Q9 Is there a label or target associated with each instance? *If so, please provide a description.*

- Yes, the primary labels are the **pairwise spatial relationship labels**. For each annotated pair of sparse points in an ambiguous region of an RGB image, there are two labels indicating the spatial relationship (depth order) between the points in two layers: one for the region ‘on’ and another for the region ‘behind’ the transparent object. The labels are ‘above’ and ‘behind’.

Q10 Is any information missing from individual instances? *If so, please provide a description, explaining why this information is missing (e.g., because it*

was unavailable). This does not include intentionally removed information, but might include, e.g., redacted text.

- No, all instances are fully annotated with RGB images, segmentation masks, and spatial relationship labels.

Q11 Are relationships between individual instances made explicit (e.g., users’ movie ratings, social network links)? *If so, please describe how these relationships are made explicit.*

- The instances are related by their source dataset, GDD [25]. All images are selected from GDD and share the characteristics of scenes within that dataset. Furthermore, images are implicitly related by the common theme of containing ambiguous regions and transparent objects, as this was the selection criterion.

Q12 Are there recommended data splits (e.g., training, development/validation, testing)? *If so, please provide a description of these splits, explaining the rationale behind them.*

- No, we do not provide predefined data splits. Users are free to define their own splits based on their specific research needs. Common splits like training/validation/testing can be created randomly or based on scene characteristics if desired.

Q13 Are there any errors, sources of noise, or redundancies in the dataset? *If so, please provide a description.*

- We have implemented a rigorous annotation pipeline, including multi-round verification by expert annotators, to minimize errors and noise in the spatial relationship labels. However, as with any human annotation, there might be minor inconsistencies or subjective interpretations. We believe the overall quality of the annotations is high due to the careful curation process. Redundancies are not intentionally introduced.

Q14 Is the dataset self-contained, or does it link to or otherwise rely on external resources (e.g., websites, tweets, other datasets)? *If it links to or relies on external resources, a) are there guarantees that they will exist, and remain constant, over time; b) are there official archival versions of the complete dataset (i.e., including the external resources as they existed at the time the dataset was created); c) are there any restrictions (e.g., licenses, fees) associated with any of the external resources that might apply to a future user? Please provide descriptions of all external resources and any restrictions associated with them, as well as links or other access points, as appropriate.*

- The MD-3k benchmark is distributed as a self-

contained dataset of annotations, segmentation masks, and image lists. It relies on the images from the GDD dataset [25] as the underlying visual data. Users will need to obtain the GDD dataset separately to use MD-3k fully.

- a) We cannot guarantee the long-term availability of the GDD dataset. However, GDD is a publicly available dataset for research purposes.
- b) We do not provide archival versions of the GDD dataset. Users should refer to the original GDD dataset sources for archival information.
- c) Users should adhere to the licensing terms of the GDD dataset, which are separate from the MD-3k benchmark license. Please refer to the GDD dataset documentation for details on licenses and restrictions.

Q15 Does the dataset contain data that might be considered confidential (e.g., data that is protected by legal privilege or by doctor-patient confidentiality, data that includes the content of individuals' non-public communications)? If so, please provide a description.

- No, the MD-3k benchmark utilizes images from the publicly available GDD dataset, which does not contain confidential information.

Q16 Does the dataset contain data that, if viewed directly, might be offensive, insulting, threatening, or might otherwise cause anxiety? If so, please describe why.

- No, the images in the MD-3k benchmark depict common indoor and outdoor scenes and do not contain offensive, insulting, threatening, or anxiety-inducing content to the best of our knowledge.

Q17 Does the dataset relate to people? If not, you may skip the remaining questions in this section.

- No. This dataset primarily focuses on scenes and spatial relationships, and does not directly relate to people in a way that raises privacy or ethical concerns. While people may be present in some images as part of the general scene context, the annotations and benchmark tasks are not centered around individuals.

Q18 Does the dataset identify any subpopulations (e.g., by age, gender)?

- N/A.

Q19 Is it possible to identify individuals (i.e., one or more natural persons), either directly or indirectly (i.e., in combination with other data) from the dataset? If so, please describe how.

- N/A.

Q20 Does the dataset contain data that might be considered sensitive in any way (e.g., data that reveals racial or ethnic origins, sexual orientations,

religious beliefs, political opinions or union memberships, or locations; financial or health data; biometric or genetic data; forms of government identification, such as social security numbers; criminal history)? If so, please provide a description.

- No.

Q21 Any other comments?

- We encourage users to exercise discretion and use the benchmark responsibly for research purposes only.

D.3. Collection Process

Q22 How was the data associated with each instance acquired? Was the data directly observable (e.g., raw text, movie ratings), reported by subjects (e.g., survey responses), or indirectly inferred/derived from other data (e.g., part-of-speech tags, model-based guesses for age or language)? If data was reported by subjects or indirectly inferred/derived from other data, was the data validated/verified? If so, please describe how.

- The RGB images were directly observable, sourced from the GDD segmentation dataset [25]. The segmentation masks and spatial relationship labels were indirectly derived through expert human annotation. Expert annotators manually identified ambiguous regions and provided pairwise spatial relationship labels. The annotations were validated through a multi-round verification process involving multiple annotators to ensure consistency and accuracy.

Q23 What mechanisms or procedures were used to collect the data (e.g., hardware apparatus or sensor, manual human curation, software program, software API)? How were these mechanisms or procedures validated?

- The data collection process primarily involved **manual human curation**. Expert annotators used in-house annotation tools to:
 - Visually inspect RGB images from the GDD dataset.
 - Identify and segment ambiguous regions, particularly those involving transparent objects, creating segmentation masks.
 - Select sparse point pairs within these ambiguous regions.
 - Determine and assign pairwise spatial relationship labels ('above' and 'behind') for each pair, considering both layers ('on' and 'behind' the transparent object).

The annotation procedure was validated through a multi-round verification process. Different annotators reviewed and cross-validated annotations to

resolve discrepancies and ensure consistency and accuracy of the labels.

Q24 If the dataset is a sample from a larger set, what was the sampling strategy (e.g., deterministic, probabilistic with specific sampling probabilities)?

- The sampling strategy was **deterministic and targeted**. Images were selected from the GDD dataset based on a specific criterion: the presence of ambiguous regions, especially those featuring transparent objects. This was a deliberate selection process to focus the benchmark on the challenges of multi-layer spatial understanding in such complex scenes, rather than a random or probabilistic sampling of the entire GDD dataset.

Q25 Who was involved in the data collection process (e.g., students, crowdworkers, contractors) and how were they compensated (e.g., how much were crowdworkers paid)?

- The data collection process involved **expert annotators**. These were individuals with expertise in computer vision and image annotation, specifically trained for the task of identifying ambiguous regions and determining spatial relationships. Compensation details are proprietary to [Anonymous Author] and are not disclosed for anonymity purposes.

Q26 Over what timeframe was the data collected? Does this timeframe match the creation timeframe of the data associated with the instances (e.g., recent crawl of old news articles)? *If not, please describe the timeframe in which the data associated with the instances was created.*

- The data annotation and collection process took place between [Anonymous Month, Year] and [Anonymous Month, Year]. This timeframe represents the creation timeframe of the segmentation masks and spatial relationship labels associated with the images from the GDD dataset. The GDD dataset itself was created prior to this timeframe.

Q27 Were any ethical review processes conducted (e.g., by an institutional review board)? *If so, please provide a description of these review processes, including the outcomes, as well as a link or other access point to any supporting documentation.*

- Ethical review processes were not formally conducted by an institutional review board specifically for the creation of MD-3k. However, the benchmark utilizes publicly available images from the GDD dataset, which is intended for research purposes. We have taken care to ensure that the annotation process and the resulting benchmark do not raise ethical concerns regarding privacy or

sensitive information.

Q28 Does the dataset relate to people? *If not, you may skip the remaining questions in this section.*

- No.

Q29 Did you collect the data from the individuals in question directly, or obtain it via third parties or other sources (e.g., websites)?

- N/A.

Q30 Were the individuals in question notified about the data collection? *If so, please describe (or show with screenshots or other information) how notice was provided, and provide a link or other access point to, or otherwise reproduce, the exact language of the notification itself.*

- N/A.

Q31 Did the individuals in question consent to the collection and use of their data? *If so, please describe (or show with screenshots or other information) how consent was requested and provided, and provide a link or other access point to, or otherwise reproduce, the exact language to which the individuals consented.*

- N/A.

Q32 If consent was obtained, were the consenting individuals provided with a mechanism to revoke their consent in the future or for certain uses? *If so, please provide a description, as well as a link or other access point to the mechanism (if appropriate).*

- N/A.

Q33 Has an analysis of the potential impact of the dataset and its use on data subjects (e.g., a data protection impact analysis) been conducted? *If so, please provide a description of this analysis, including the outcomes, as well as a link or other access point to any supporting documentation.*

- No formal data protection impact analysis has been conducted. However, as the dataset does not directly relate to people and uses publicly available images, we anticipate minimal risk to data subjects. The focus of the benchmark is on evaluating computer vision models for spatial understanding. We encourage responsible use of the benchmark for research purposes.

Q34 Any other comments?

- No.

D.4. Preprocessing, Cleaning, and/or Labeling

Q35 Was any preprocessing/cleaning/labeling of the data done (e.g., discretization or bucketing, tokenization, part-of-speech tagging, SIFT feature extraction, removal of instances, processing of missing values)? *If so, please provide a description.*

If not, you may skip the remainder of the questions in this section.

- Yes, **labeling** was performed. Expert annotators manually labeled spatial relationships for pairs of sparse points in ambiguous regions. This labeling process is the core contribution of the MD-3k benchmark. No other preprocessing or cleaning of the RGB images from the GDD dataset was performed.

Q36 Was the “raw” data saved in addition to the pre-processed/cleaned/labeled data (e.g., to support anticipated future uses)? *If so, please provide a link or other access point to the “raw” data.*

- N/A. The ‘raw’ data in this context would be the original RGB images from the GDD dataset. We are distributing the segmentation masks and spatial relationship labels, which are the ‘labeled’ data. The ‘raw’ RGB images are available from the original GDD dataset [25].

Q37 Is the software used to preprocess/clean/label the instances available? *If so, please provide a link or other access point.*

- The in-house annotation tools used for labeling are not publicly released at this time due to proprietary reasons. However, we will provide detailed descriptions of the annotation process and data format to facilitate the use of the benchmark.

Q38 Any other comments?

- No.

D.5. Uses

Q39 Has the dataset been used for any tasks already? *If so, please provide a description.*

- Not yet. MD-3k is a newly introduced benchmark. We will present initial baseline evaluations in our paper.

Q40 Is there a repository that links to any or all papers or systems that use the dataset? *If so, please provide a link or other access point.*

- We will maintain a repository at [Anonymous Repo] that links to papers and systems that utilize the MD-3k benchmark as they become available.

Q41 What (other) tasks could the dataset be used for?

- The primary intended use of MD-3k is for evaluating models for **multi-layer spatial understanding** and **depth disentanglement** in ambiguous scenes. Specifically, it can be used to:
 - Evaluate the performance of depth estimation models in regions with transparency and complex spatial arrangements.
 - Benchmark algorithms designed for understanding layered scene representations.

- Analyze the ability of models to reason about relative depth ordering in multi-layer contexts.
- Develop and test novel approaches for handling spatial ambiguity in 3D scene understanding.

It can also be used for related tasks such as transparent object segmentation and reasoning about spatial relationships in general.

Q42 Is there anything about the composition of the dataset or the way it was collected and pre-processed/cleaned/labeled that might impact future uses? *For example, is there anything that a future user might need to know to avoid uses that could result in unfair treatment of individuals or groups (e.g., stereotyping, quality of service issues) or other undesirable harms (e.g., financial harms, legal risks)?* *If so, please provide a description. Is there anything a future user could do to mitigate these undesirable harms?*

- The MD-3k benchmark is focused on ambiguous scenes, particularly those with transparent objects. Users should be aware that the dataset is specifically designed to challenge models in these scenarios. It might not be representative of general scenes without ambiguity. Future users should consider this focus when applying the benchmark and interpreting results. As the dataset does not relate to people or sensitive attributes, the risk of unfair treatment or other harms is considered low. However, responsible and ethical use of the benchmark is always encouraged.

Q43 Are there tasks for which the dataset should not be used? *If so, please provide a description.*

- We are not aware of any specific tasks for which MD-3k should not be used. However, its primary focus is on multi-layer spatial understanding in ambiguous regions. Using it for tasks completely unrelated to spatial reasoning or depth perception might not be appropriate.

Q44 Any other comments?

- No.

D.6. Distribution and License

Q45 Will the dataset be distributed to third parties outside of the entity (e.g., company, institution, organization) on behalf of which the dataset was created? *If so, please provide a description.*

- Yes, the MD-3k benchmark will be publicly distributed to third parties for research purposes.

Q46 How will the dataset be distributed (e.g., tarball on website, API, GitHub)? *Does the dataset have a digital object identifier (DOI)?*

- The MD-3k benchmark, including annotations, segmentation masks, and code for evaluation,

will be distributed as a downloadable tarball via [Anonymous Repo], likely a GitHub repository. We plan to obtain a DOI for the benchmark upon publication of the associated paper.

Q47 When will the dataset be distributed?

- We plan to distribute the dataset publicly starting from March, 2025, and onwards, coinciding with the anticipated publication of our work.

Q48 Will the dataset be distributed under a copyright or other intellectual property (IP) license, and/or under applicable terms of use (ToU)? If so, please describe this license and/or ToU, and provide a link or other access point to, or otherwise reproduce, any relevant licensing terms or ToU, as well as any fees associated with these restrictions.

- The MD-3k benchmark, including annotations and code, will be released under the **Apache-2.0 license**. This is an open-source license that allows for free use, modification, and distribution for research and commercial purposes, with proper attribution. The full license text will be available in the benchmark repository at [Anonymous Repo]. There are no fees associated with the use of the MD-3k benchmark under this license.

Q49 Have any third parties imposed IP-based or other restrictions on the data associated with the instances? If so, please describe these restrictions, and provide a link or other access point to, or otherwise reproduce, any relevant licensing terms, as well as any fees associated with these restrictions.

- The MD-3k benchmark relies on RGB images from the GDD dataset [25]. Users of MD-3k should also comply with the licensing terms of the GDD dataset, which are separate from the Apache-2.0 license of our benchmark. We recommend users refer to the GDD dataset documentation for details on their specific licensing terms and any potential restrictions. We are not aware of any IP-based or other restrictions imposed by third parties directly on our annotations and benchmark data, other than the underlying GDD images.

Q50 Do any export controls or other regulatory restrictions apply to the dataset or to individual instances? If so, please describe these restrictions, and provide a link or other access point to, or otherwise reproduce, any supporting documentation.

- No, we are not aware of any export controls or other regulatory restrictions applicable to the MD-3k benchmark or its individual instances.

Q51 Any other comments?

- No.

D.7. Maintenance

Q52 Who will be supporting/hosting/maintaining the dataset?

- Anonymous Author will be responsible for supporting, hosting, and maintaining the MD-3k benchmark.

Q53 How can the owner/curator/manager of the dataset be contacted (e.g., email address)?

- The owner/curator/manager of the dataset can be contacted through [Anonymous Contact Method], which will be provided in the benchmark repository at [Anonymous Repo] upon release.

Q54 Is there an erratum? If so, please provide a link or other access point.

- There is no erratum for the initial release of MD-3k. Any errata identified in the future will be documented and communicated through the benchmark repository at [Anonymous Repo].

Q55 Will the dataset be updated (e.g., to correct labeling errors, add new instances, delete instances)? If so, please describe how often, by whom, and how updates will be communicated to users (e.g., mailing list, GitHub)?

- Yes, we plan to update the MD-3k benchmark periodically. Updates may include corrections of labeling errors, addition of new instances, or improvements to the benchmark resources. Updates will be performed by [Anonymous Author] and will be communicated to users through the benchmark repository at [Anonymous Repo], potentially via release notes and/or announcements on the repository's issue tracker.

Q56 If the dataset relates to people, are there applicable limits on the retention of the data associated with the instances (e.g., were individuals in question told that their data would be retained for a fixed period of time and then deleted)? If so, please describe these limits and explain how they will be enforced.

- N/A.

Q57 Will older versions of the dataset continue to be supported/hosted/maintained? If so, please describe how. If not, please describe how its obsolescence will be communicated to users.

- We intend to host and maintain older versions of the MD-3k benchmark in the benchmark repository at [Anonymous Repo], likely through version control mechanisms (e.g., Git tags or branches). This will allow users to access and utilize specific versions of the benchmark for reproducibility and comparison purposes. If a version becomes obsolete, it will be clearly marked as such in the repository, but will remain accessible.

Q58 If others want to extend/augment/build on/contribute to the dataset, is there a mechanism for them to do so? *If so, please provide a description. Will these contributions be validated/verified? If so, please describe how. If not, why not? Is there a process for communicating/distributing these contributions to other users? If so, please provide a description.*

- We welcome contributions from the community to extend, augment, or build upon the MD-3k benchmark. Users can contribute by:
 - Reporting issues or suggesting improvements via the issue tracker in the benchmark repository at [Anonymous Repo].
 - Submitting pull requests with code contributions (e.g., evaluation scripts, new baselines).
 - Proposing new annotations or extensions to the dataset by contacting [Anonymous Author] through the contact method provided in the repository.

Q59 Any other comments?

- No.

E. Broader Impact

This work transcends monocular depth estimation, tackling the fundamental challenge of depth ambiguity that limits spatial understanding across AI. By resolving this core limitation, we pave the way for more reliable and versatile AI in complex 3D environments, impacting diverse fields reliant on robust perception.

Our central contribution, Laplacian Visual Prompting (LVP), introduces a training-free spectral technique. LVP empowers models to explicitly disentangle depth ambiguity and generate multi-hypothesis predictions, unlocking latent spatial knowledge. This broadly applicable spectral prompting paradigm extends beyond depth, offering a transformative tool for visual model adaptation and interpretation across tasks grappling with ambiguity and layered representations.

The MD-3k benchmark, the first of its kind with multi-layer spatial relationship labels, provides a critical platform for rigorous evaluation of multi-layer spatial understanding. MD-3k enables fine-grained analysis of depth disentanglement, pushing beyond single-layer metrics and driving progress in foundational spatial intelligence for computer vision, robotics, and AI.

Ultimately, LVP demonstrates spectral prompting as a powerful mechanism to unlock zero-shot multi-layer spatial understanding from existing models. This paradigm shift towards spectral prompting and multi-hypothesis spatial foundation models opens transformative avenues for interpretable, adaptable, and robust AI. By conquering depth ambiguity, this research delivers essential tools

and insights for building foundational models capable of truly understanding real-world 3D scenes.

F. Availability and Maintenance

To accelerate progress in multi-layer spatial understanding and spectral prompting, all code and datasets from this study are publicly released at [Anonymous Repo]. This repository provides:

- **Laplacian Visual Prompting (LVP) code.** Ready-to-use implementation for spectral prompting.
- **MD-3k benchmark.** The first multi-layer spatial relationship dataset for rigorous evaluation.
- **Evaluation suite and baselines.** Code to reproduce and extend our experimental results.
- **Reproduction guide.** Step-by-step instructions for full experiment replication.

We are committed to the sustained accessibility and usability of these resources, empowering the community to build upon this foundation and drive future innovations in ambiguity-free spatial AI. We actively encourage researchers to leverage MD-3k and LVP to advance the state-of-the-art in spatial understanding.

G. License

The MD-3k benchmark and the Laplacian Visual Prompting code are released under the Apache License 2.0.

H. Public Resources Used

We acknowledge the following public resources used in this work:

- Depth-Anything-v2⁶ ... Apache-2.0+CC-BY-NC-4.0
- Depth-Anything⁷ Apache-2.0
- DPT⁸ MIT
- ZoeDepth⁹ MIT
- Marigold¹⁰ Apache-2.0
- GeoWizard¹¹ CC BY 4.0
- Diffusers¹² Apache-2.0
- Video Depth Anything¹³ Apache-2.0

⁶<https://github.com/DepthAnything/Depth-Anything-V2>

⁷<https://github.com/LiheYoung/Depth-Anything>.

⁸<https://github.com/isl-org/DPT>.

⁹<https://github.com/isl-org/ZoeDepth>.

¹⁰<https://github.com/prs-eth/Marigold>.

¹¹<https://github.com/fuxiao0719/GeoWizard>.

¹²<https://github.com/huggingface/diffusers/tree/main>

¹³<https://github.com/DepthAnything/Video-Depth-Anything>

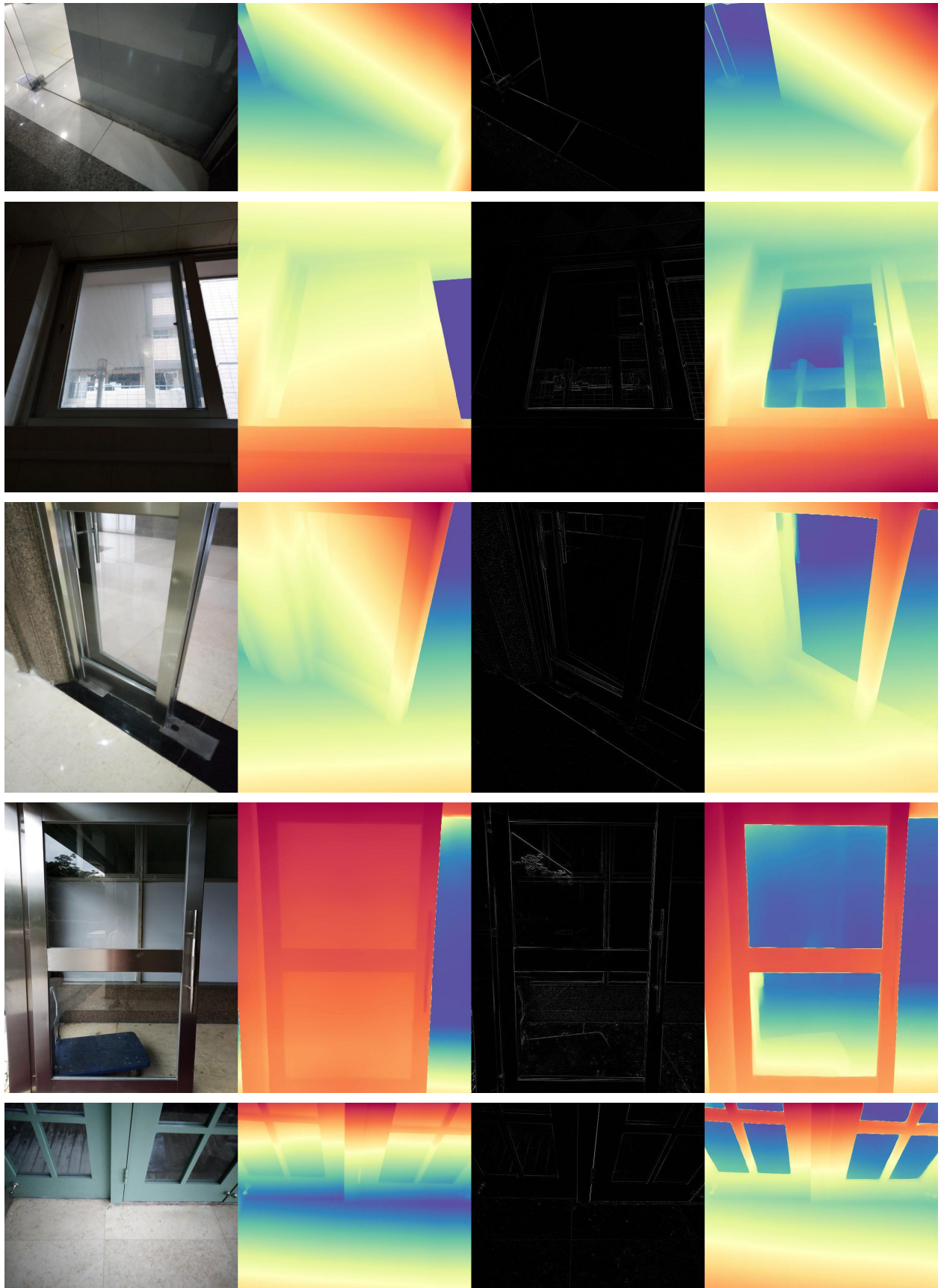


Figure E. **LVP-empowered multi-layer depth.** Each case includes an RGB image with its depth, and the Laplacian with its depth.

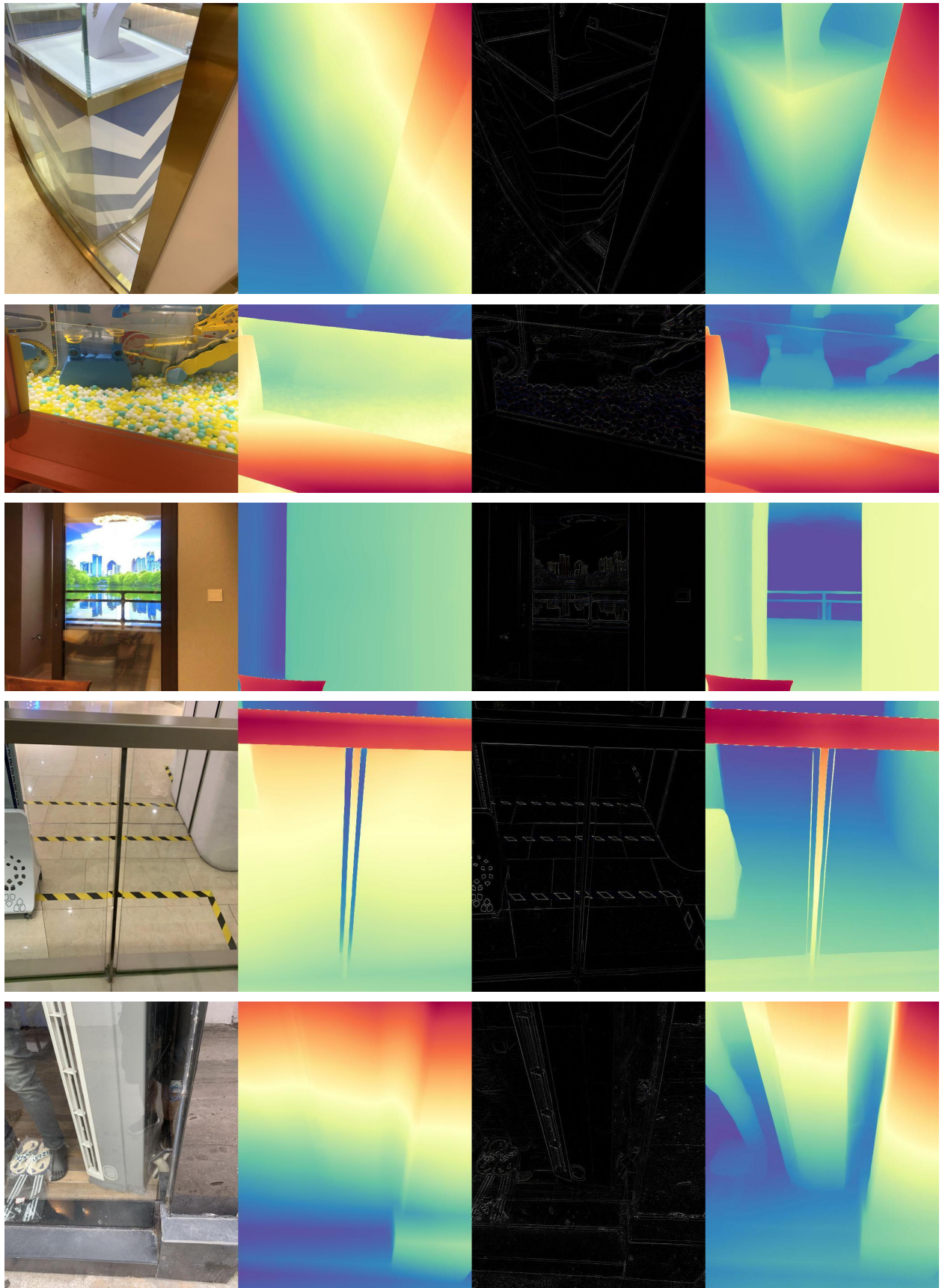


Figure F. **LVP-empowered multi-layer depth.** Each case includes an RGB image with its depth, and the Laplacian with its depth.

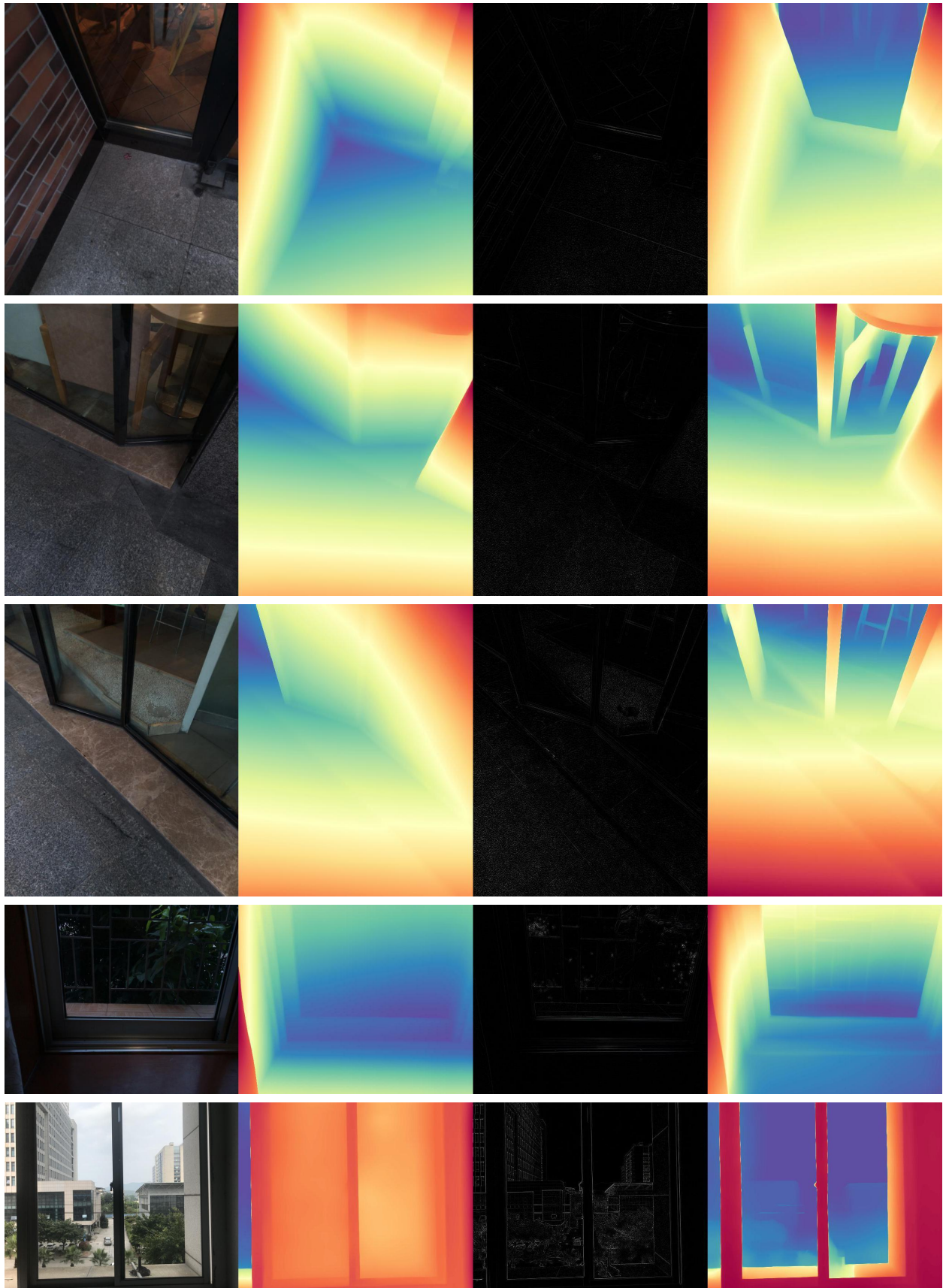


Figure G. LVP-empowered multi-layer depth. Each case includes an RGB image with its depth, and the Laplacian with its depth.

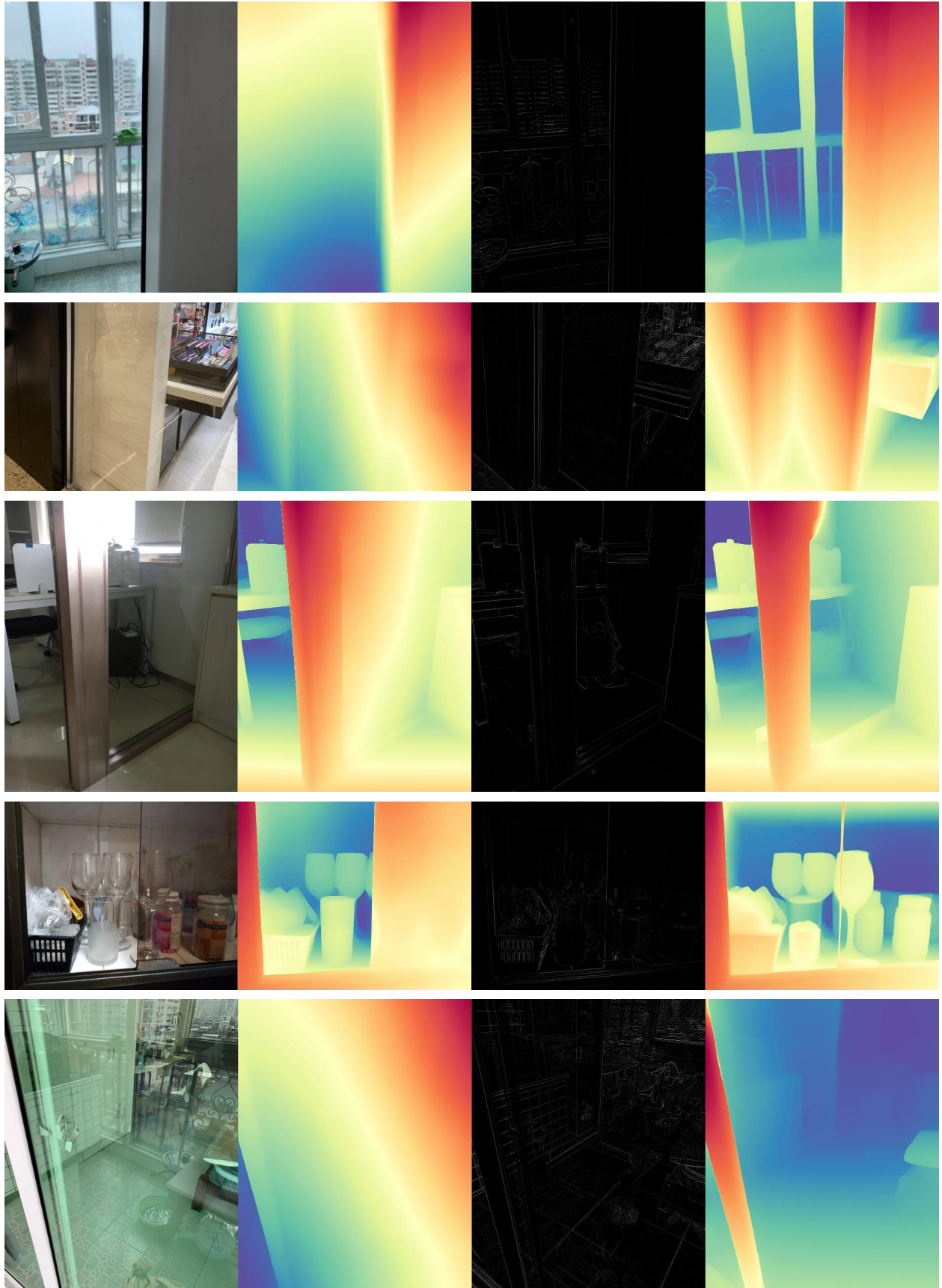


Figure H. LVP-empowered multi-layer depth. Each case includes an RGB image with its depth, and the Laplacian with its depth.

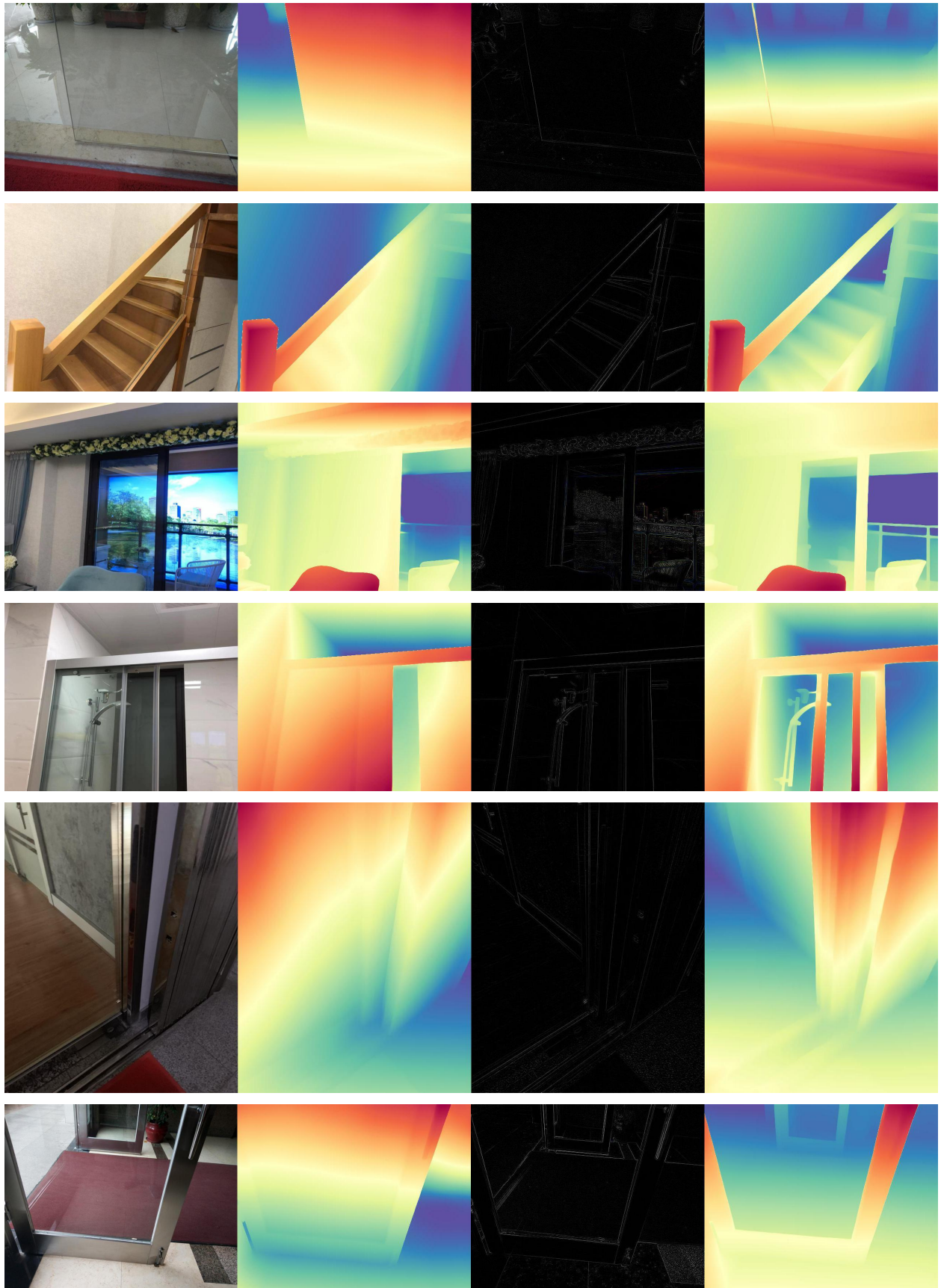


Figure 1. **LVP-empowered multi-layer depth.** Each case includes an RGB image with its depth, and the Laplacian with its depth.

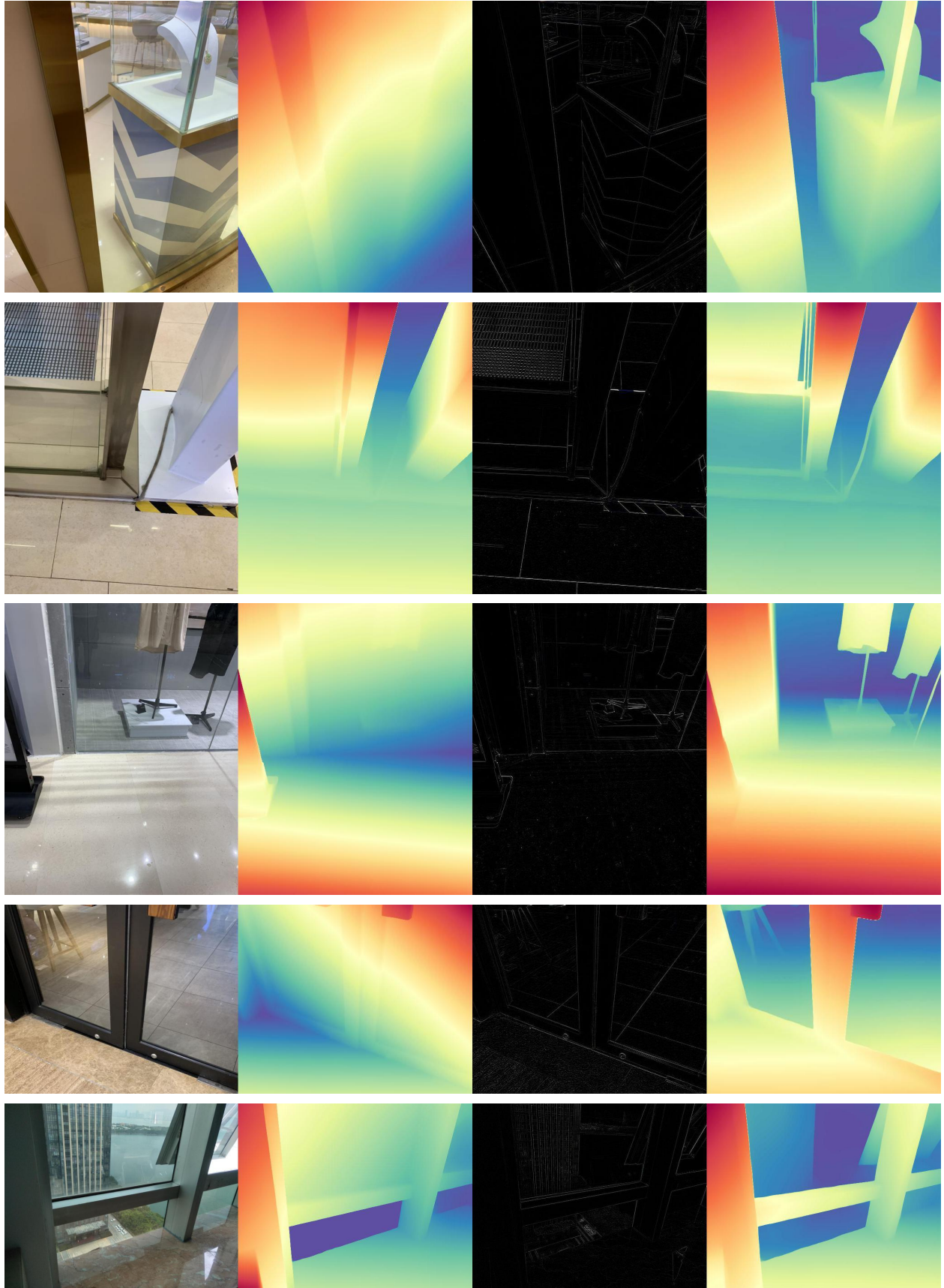


Figure J. LVP-empowered multi-layer depth. Each case includes an RGB image with its depth, and the Laplacian with its depth.

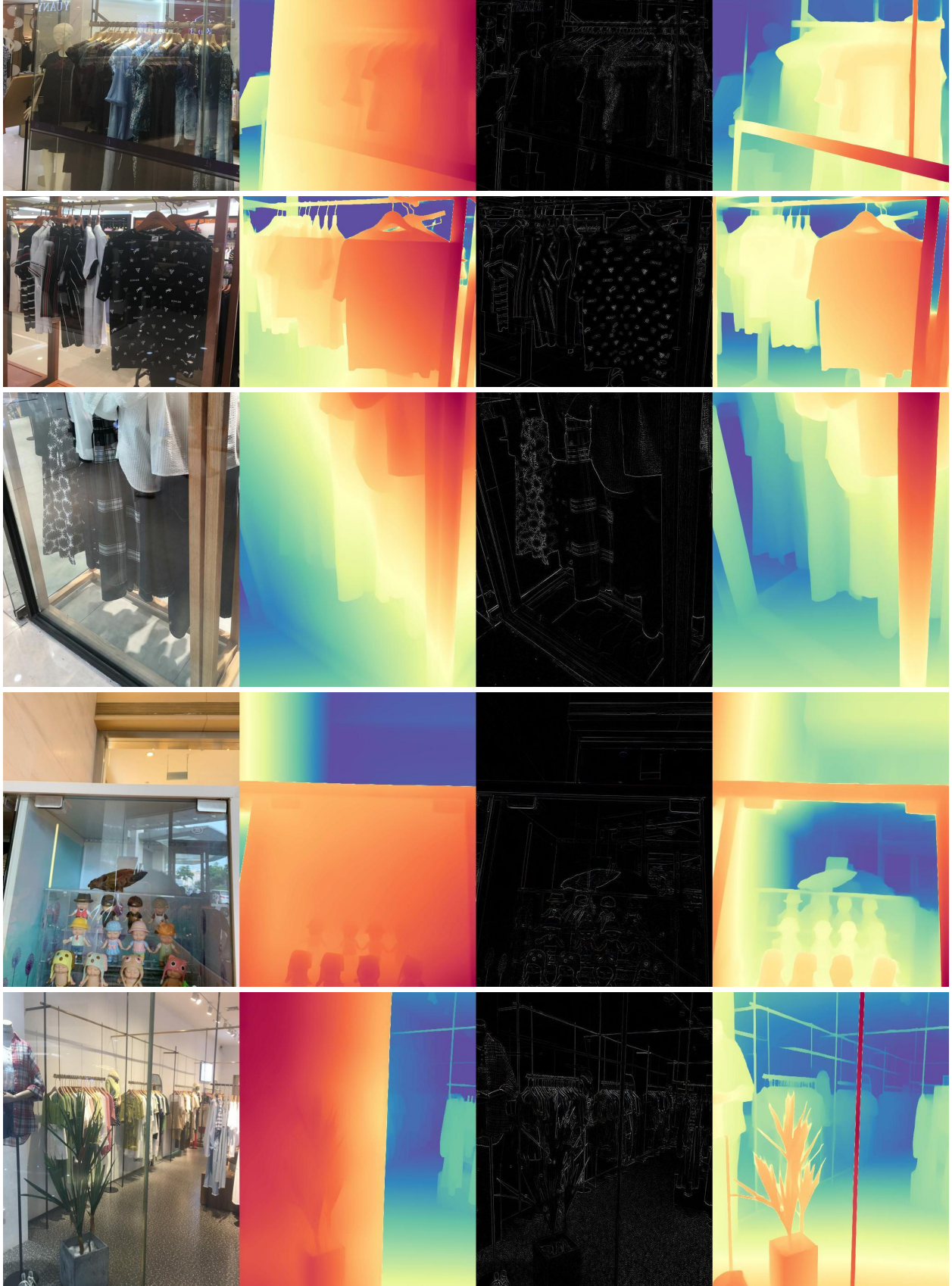


Figure K. **Failure cases** of multi-layer depth estimation via Laplacian Visual Prompting. Each case shows the RGB input, the estimated depth via RGB, the Laplacian input, and the estimated *depth* via Laplacian input.

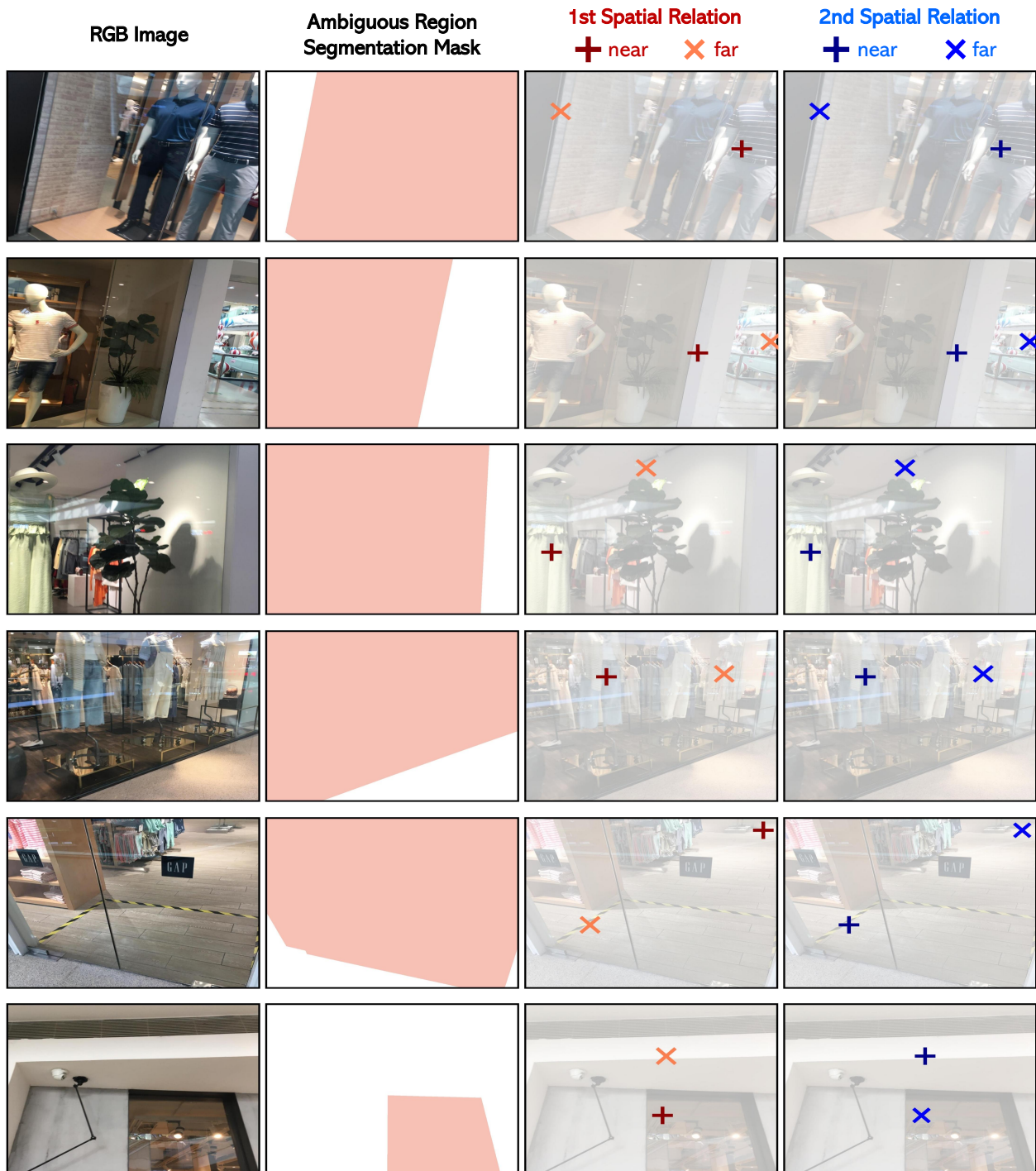


Figure L. MD-3k benchmark for evaluating multi-layer spatial relationships. Example images with annotated sparse point pairs are shown, illustrating ambiguous regions and relative depth relationships. The first and second spatial relation columns show ground truth annotations for near/far relationships between layers, using red and blue markers, respectively.

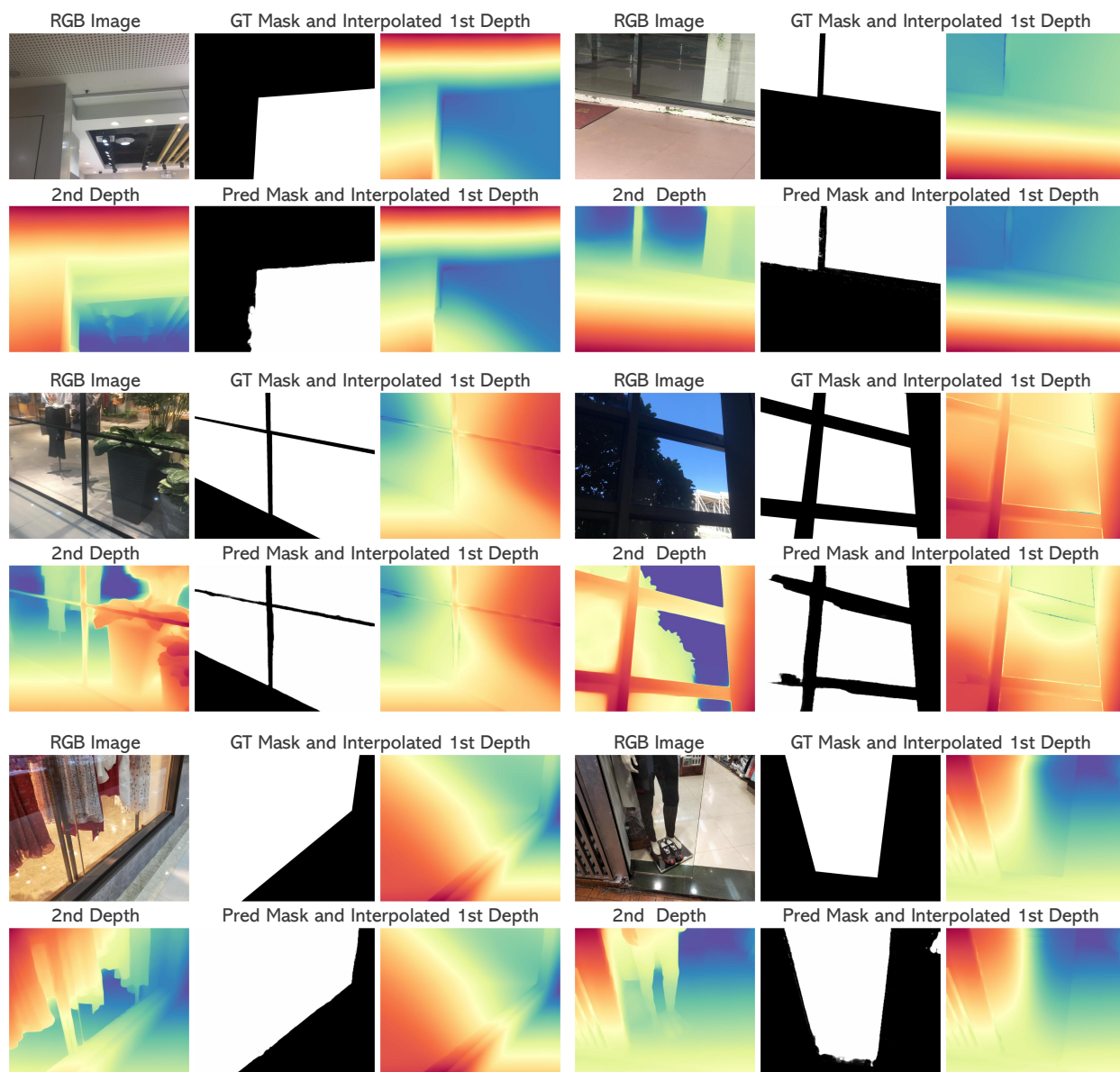


Figure M. Multi-layer depth with extra semantic prior (successful cases).

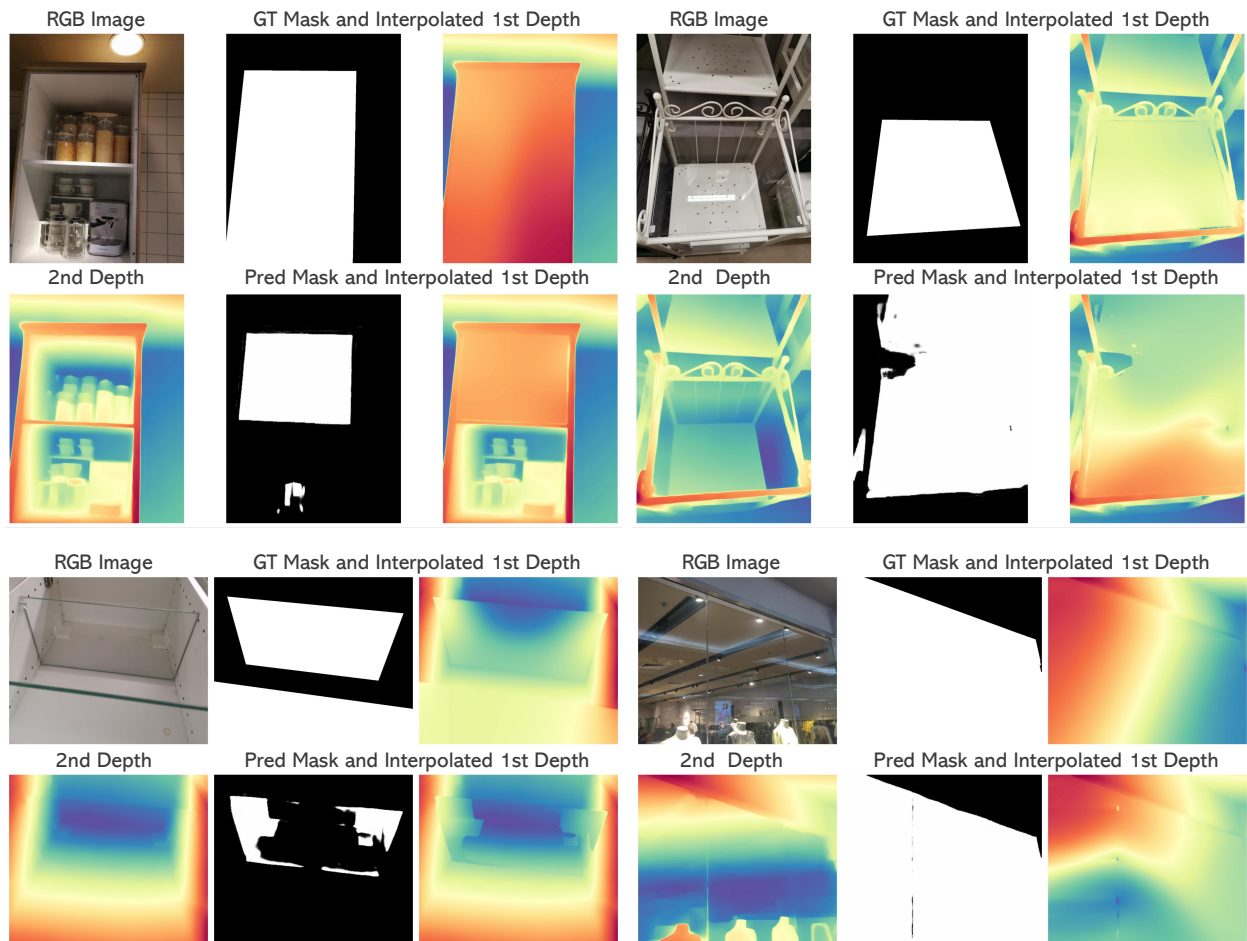


Figure N. Multi-layer depth with extra semantic prior (failure cases).

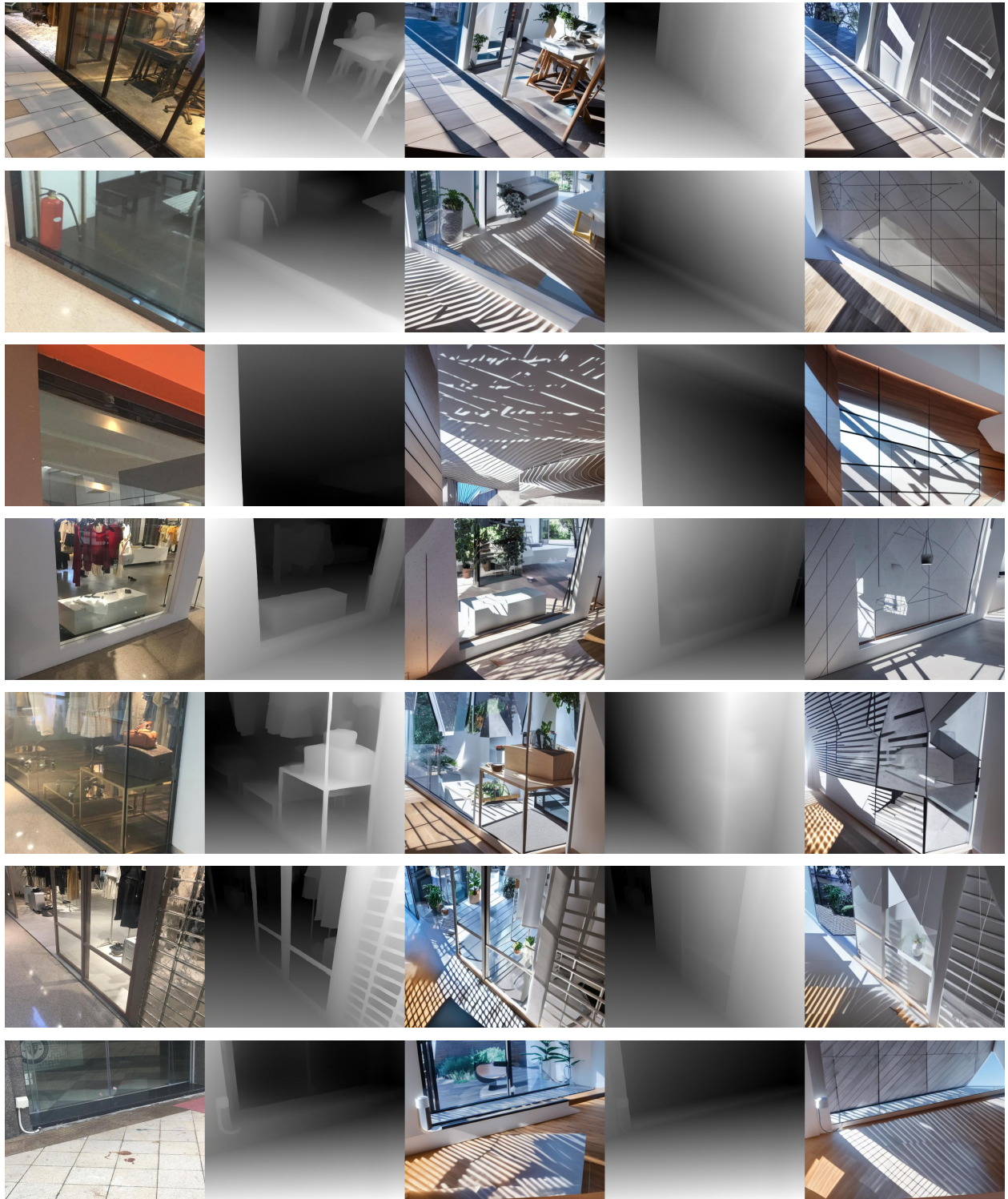


Figure O. **Multi-hypothesis spatial understanding enhances flexible geometry-conditioned visual generation.** From left to right: original RGB image, depth from Laplacian Visual Prompting with its corresponding generated RGB image, and depth from the original RGB image with its generated RGB counterpart.

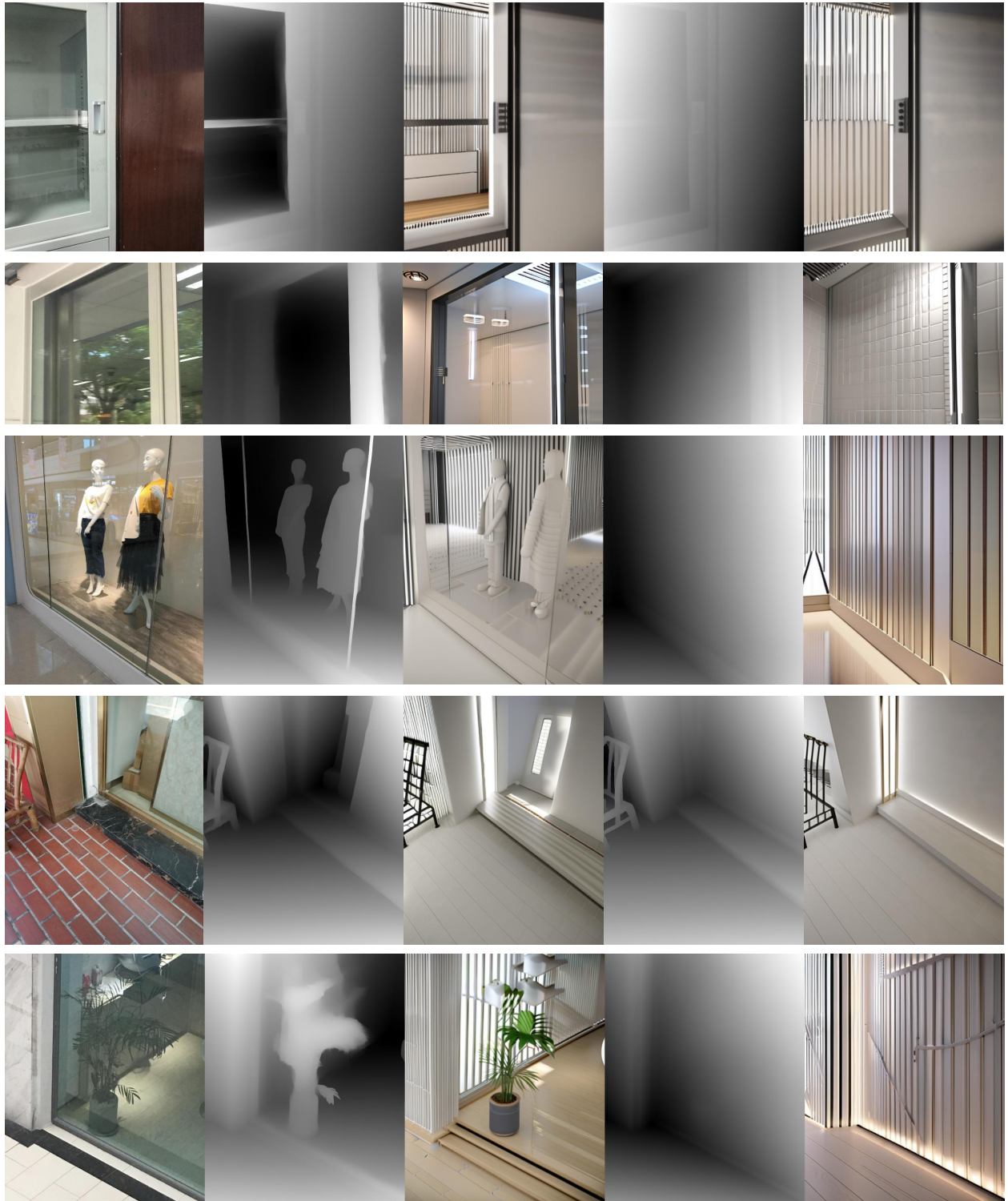


Figure P. **Multi-hypothesis spatial understanding enhances flexible geometry-conditioned visual generation.** From left to right: original RGB image, depth from Laplacian Visual Prompting with its corresponding generated RGB image, and depth from the original RGB image with its generated RGB counterpart.

References

- [1] Hyojin Bahng, Ali Jahanian, Swami Sankaranarayanan, and Phillip Isola. Exploring visual prompts for adapting large-scale models. *arXiv preprint arXiv:2203.17274*, 1(3):4, 2022. 3
- [2] Yutong Bai, Xinyang Geng, Karttikeya Mangalam, Amir Bar, Alan L Yuille, Trevor Darrell, Jitendra Malik, and Alexei A Efros. Sequential modeling enables scalable learning for large vision models. In *CVPR*, pages 22861–22872, 2024. 2, 3, 7
- [3] Amir Bar, Yossi Gandelsman, Trevor Darrell, Amir Globerson, and Alexei Efros. Visual prompting via image inpainting. *NeurIPS*, 35:25005–25017, 2022. 2
- [4] Shariq Farooq Bhat, Ibraheem Alhashim, and Peter Wonka. Adabins: Depth estimation using adaptive bins. In *CVPR*, 2021. 3
- [5] Shariq Farooq Bhat, Reiner Birkel, Diana Wofk, Peter Wonka, and Matthias Müller. Zoedepth: Zero-shot transfer by combining relative and metric depth. *arXiv:2302.12288*, 2023. 2, 5
- [6] Reiner Birkel, Diana Wofk, and Matthias Müller. Midas v3. 1—a model zoo for robust monocular relative depth estimation. *arXiv:2307.14460*, 2023. 2, 3
- [7] Tom Brown, Benjamin Mann, Nick Ryder, Melanie Subbiah, Jared D Kaplan, Prafulla Dhariwal, Arvind Nee-lakantan, Pranav Shyam, Girish Sastry, Amanda Askell, et al. Language models are few-shot learners. *NeurIPS*, 33:1877–1901, 2020. 3
- [8] Aochuan Chen, Peter Lorenz, Yuguang Yao, Pin-Yu Chen, and Sijia Liu. Visual prompting for adversarial robustness. In *ICASSP*, pages 1–5. IEEE, 2023. 3
- [9] Lingwei Chen, Yujie Fan, and Yanfang Ye. Adversarial reprogramming of pretrained neural networks for fraud detection. In *CIKM*, pages 2935–2939, 2021. 3
- [10] Weifeng Chen, Zhao Fu, Dawei Yang, and Jia Deng. Single-image depth perception in the wild. In *NeurIPS*, 2016. 3
- [11] David Eigen, Christian Puhersch, and Rob Fergus. Depth map prediction from a single image using a multi-scale deep network. In *NeurIPS*, 2014. 3
- [12] Lijie Fan, Kaifeng Chen, Dilip Krishnan, Dina Katabi, Phillip Isola, and Yonglong Tian. Scaling laws of synthetic images for model training... for now. In *CVPR*, pages 7382–7392, 2024. 7
- [13] Huan Fu, Mingming Gong, Chaohui Wang, Kayhan Bat-manghelich, and Dacheng Tao. Deep ordinal regression network for monocular depth estimation. In *CVPR*, 2018. 3
- [14] Xiao Fu, Wei Yin, Mu Hu, Kaixuan Wang, Yuexin Ma, Ping Tan, Shaojie Shen, Dahua Lin, and Xiaoxiao Long. Geowizard: Unleashing the diffusion priors for 3d geometry estimation from a single image. *ECCV*, 2024. 2, 3, 5
- [15] Timnit Gebru, Jamie Morgenstern, Briana Vecchione, Jennifer Wortman Vaughan, Hanna Wallach, Hal Daumé III, and Kate Crawford. Datasheets for datasets. *Commun. ACM*, 64(12):86–92, 2021. 3, 12
- [16] Andreas Geiger, Philip Lenz, Christoph Stiller, and Raquel Urtasun. Vision meets robotics: The kitti dataset. *IJRR*, 2013. 3
- [17] Ming Gui, Johannes S Fischer, Ulrich Prestel, Pingchuan Ma, Dmytro Kotovenko, Olga Grebenkova, Stefan Andreas Baumann, Vincent Tao Hu, and Björn Ommer. Depthfm: Fast monocular depth estimation with flow matching. *arXiv:2403.13788*, 2024. 2, 3
- [18] Vitor Guizilini, Igor Vasiljevic, Dian Chen, Rareş Ambruş, and Adrien Gaidon. Towards zero-shot scale-aware monocular depth estimation. In *ICCV*, 2023. 2
- [19] Alberto Hojel, Yutong Bai, Trevor Darrell, Amir Globerson, and Amir Bar. Finding visual task vectors. In *ECCV*, pages 257–273. Springer, 2025. 2
- [20] Bingxin Ke, Anton Obukhov, Shengyu Huang, Nando Metzger, Rodrigo Caye Daudt, and Konrad Schindler. Repurposing diffusion-based image generators for monocular depth estimation. In *CVPR*, 2024. 2, 3, 5, 9
- [21] Muhammad Uzair Khattak, Hanoona Rasheed, Muhammad Maaz, Salman Khan, and Fahad Shahbaz Khan. Maple: Multi-modal prompt learning. *CVPR*, 2023. 3
- [22] Zhenyu Li, Shariq Farooq Bhat, and Peter Wonka. Patchfusion: An end-to-end tile-based framework for high-resolution monocular metric depth estimation. In *CVPR*, 2024. 2
- [23] Yuan Liang, Bailin Deng, Wenxi Liu, Jing Qin, and Shengfeng He. Monocular depth estimation for glass walls with context: a new dataset and method. *TPAMI*, 2023. 12
- [24] Jiaying Lin, Zebang He, and Rynson WH Lau. Rich context aggregation with reflection prior for glass surface detection. In *CVPR*, pages 13415–13424, 2021. 10
- [25] Haiyang Mei, Xin Yang, Yang Wang, Yuanyuan Liu, Shengfeng He, Qiang Zhang, Xiaopeng Wei, and Rynson WH Lau. Don’t hit me! glass detection in real-world scenes. In *CVPR*, pages 3687–3696, 2020. 3, 13, 14, 16, 17
- [26] Paarth Neekhara, Shehzeen Hussain, Jinglong Du, Shlomo Dubnov, Farinaz Koushanfar, and Julian McAuley. Cross-modal adversarial reprogramming. In *WACV*, pages 2427–2435, 2022. 3
- [27] Luigi Piccinelli, Yung-Hsu Yang, Christos Sakaridis, Mattia Segu, Siyuan Li, Luc Van Gool, and Fisher Yu. Unidepth: Universal monocular metric depth estimation. In *CVPR*, 2024. 2
- [28] René Ranftl, Alexey Bochkovskiy, and Vladlen Koltun. Vision transformers for dense prediction. In *ICCV*, 2021. 2, 3, 5, 9
- [29] René Ranftl, Katrin Lasinger, David Hafner, Konrad Schindler, and Vladlen Koltun. Towards robust monocular depth estimation: Mixing datasets for zero-shot cross-dataset transfer. *TPAMI*, 2022. 2, 3
- [30] Robin Rombach, Andreas Blattmann, Dominik Lorenz, Patrick Esser, and Björn Ommer. High-resolution image synthesis with latent diffusion models. In *CVPR*, 2022. 3
- [31] Nathan Silberman, Derek Hoiem, Pushmeet Kohli, and Rob Fergus. Indoor segmentation and support inference from rgb-d images. In *ECCV*, 2012. 3

- [32] Mainak Singha, Harsh Pal, Ankit Jha, and Biplab Banerjee. Ad-clip: Adapting domains in prompt space using clip. In *ICCV*, pages 4355–4364, 2023. [3](#)
- [33] Megan Tjandrasuwita, Chanakya Ekbote, Liu Ziyin, and Paul Pu Liang. Understanding the emergence of multimodal representation alignment. *arXiv preprint arXiv:2502.16282*, 2025. [7](#)
- [34] Yun-Yun Tsai, Pin-Yu Chen, and Tsung-Yi Ho. Transfer learning without knowing: Reprogramming black-box machine learning models with scarce data and limited resources. *ICML*, 2020. [3](#)
- [35] Hao Wang, Fang Liu, Licheng Jiao, Jiahao Wang, Zehua Hao, Shuo Li, Lingling Li, Puhua Chen, and Xu Liu. Vilt-clip: Video and language tuning clip with multimodal prompt learning and scenario-guided optimization. In *AAAI*, pages 5390–5400, 2024. [3](#)
- [36] Syed Talal Wasim, Muzammal Naseer, Salman Khan, Fahad Shahbaz Khan, and Mubarak Shah. Vita-clip: Video and text adaptive clip via multimodal prompting. In *CVPR*, pages 23034–23044, 2023. [3](#)
- [37] Jason Wei, Xuezhi Wang, Dale Schuurmans, Maarten Bosma, Fei Xia, Ed Chi, Quoc V Le, Denny Zhou, et al. Chain-of-thought prompting elicits reasoning in large language models. *NeurIPS*, 35:24824–24837, 2022. [2](#)
- [38] Lihe Yang, Bingyi Kang, Zilong Huang, Xiaogang Xu, Jiashi Feng, and Hengshuang Zhao. Depth anything: Unleashing the power of large-scale unlabeled data. In *CVPR*, 2024. [2](#), [3](#), [5](#), [9](#), [10](#)
- [39] Lihe Yang, Bingyi Kang, Zilong Huang, Zhen Zhao, Xiaogang Xu, Jiashi Feng, and Hengshuang Zhao. Depth anything v2. *NeurIPS*, 2024. [2](#), [3](#), [5](#), [6](#), [9](#)
- [40] Wei Yin, Chi Zhang, Hao Chen, Zhipeng Cai, Gang Yu, Kaixuan Wang, Xiaozhi Chen, and Chunhua Shen. Metric3d: Towards zero-shot metric 3d prediction from a single image. In *ICCV*, 2023. [3](#)
- [41] Wei Yin, Chi Zhang, Hao Chen, Zhipeng Cai, Gang Yu, Kaixuan Wang, Xiaozhi Chen, and Chunhua Shen. Metric3d: Towards zero-shot metric 3d prediction from a single image. In *ICCV*, pages 9043–9053, 2023. [2](#)
- [42] Lvmin Zhang, Anyi Rao, and Maneesh Agrawala. Adding conditional control to text-to-image diffusion models. In *ICCV*, 2023. [2](#), [7](#)